CERN-EP/2016-004
2018/07/04

CMS-SUS-14-015

Search for direct pair production of scalar top quarks in the single- and dilepton channels in proton-proton collisions at $\sqrt{s} = 8 \text{ TeV}$

The CMS Collaboration*

Abstract

Results are reported from a search for the top squark \tilde{t}_1 , the lighter of the two supersymmetric partners of the top quark. The data sample corresponds to 19.7 fb^{-1} of proton-proton collisions at $\sqrt{s} = 8 \text{ TeV}$ collected with the CMS detector at the LHC. The search targets $\tilde{t}_1 \rightarrow b\tilde{\chi}_1^\pm$ and $\tilde{t}_1 \rightarrow t^{(*)}\tilde{\chi}_1^0$ decay modes, where $\tilde{\chi}_1^\pm$ and $\tilde{\chi}_1^0$ are the lightest chargino and neutralino, respectively. The reconstructed final state consists of jets, b jets, missing transverse energy, and either one or two leptons. Leading backgrounds are determined from data. No significant excess in data is observed above the expectation from standard model processes. The results exclude a region of the two-dimensional plane of possible \tilde{t}_1 and $\tilde{\chi}_1^0$ masses. The highest excluded \tilde{t}_1 and $\tilde{\chi}_1^0$ masses are about 700 GeV and 250 GeV, respectively.

Published in the Journal of High Energy Physics as doi:10.1007/JHEP07(2016)027.

1 Introduction

Theories of supersymmetry (SUSY) predict the existence of a scalar partner for each standard model (SM) left-handed and right-handed fermion. When the symmetry is broken, the scalar partners acquire a mass different from their SM counterparts, the mass splitting between scalar mass eigenstates being dependent on the mass of the SM fermion. Because of the large mass of the top quark, the splitting between its chiral supersymmetric partners is potentially the largest among all supersymmetric quarks (squarks). As a result the lighter supersymmetric scalar partner of the top quark, the top squark (\tilde{t}_1), could be the lightest squark. The search for a low mass top squark is of particular interest following the discovery of a Higgs boson [1–3], as a top squark with a mass in the TeV range would contribute substantially to the cancellation of the divergent loop corrections to the Higgs boson mass. SUSY scenarios with a neutralino ($\tilde{\chi}_1^0$) as lightest supersymmetric particle (LSP) and a nearly degenerate-mass \tilde{t}_1 provide one theoretically possible way to produce the observed relic abundance of dark matter [4, 5]; this further motivates the search for the \tilde{t}_1 at the LHC.

In this paper we report two searches for direct top squark pair production with the CMS detector at $\sqrt{s} = 8$ TeV with integrated luminosities of 19.5 fb^{-1} and 19.7 fb^{-1} . Each search is based on the two decay modes shown in Fig. 1. The decay modes and the nomenclature we will use to refer to them are as follows:

$$\begin{aligned} pp &\rightarrow \tilde{t}_1 \tilde{t}_1^* \rightarrow t^{(*)} \bar{t}^{(*)} \tilde{\chi}_1^0 \tilde{\chi}_1^0 && \text{(the “tt” decay mode);} \\ pp &\rightarrow \tilde{t}_1 \tilde{t}_1^* \rightarrow b \bar{b} \tilde{\chi}_1^+ \tilde{\chi}_1^- \rightarrow b \bar{b} W^{(*)} W^{(*)} \tilde{\chi}_1^0 \tilde{\chi}_1^0 && \text{(the “bbWW” decay mode).} \end{aligned}$$

The tt and bbWW events both contain bottom quark jets (henceforth called b jets) and may contain charged leptons and neutrinos from $W^{(*)}$ decay. The search strategies are therefore tailored to require either one lepton or two leptons, as well as at least one b jet and a minimum amount of transverse momentum imbalance. Throughout this paper the term “lepton” refers only to e^\pm and μ^\pm . Previous searches for low mass top squarks in leptonic final states have been conducted by the D0, CDF, CMS, and ATLAS collaborations [6–12].

As shown in Table 1, we categorize the decays of the \tilde{t}_1 as 2-body or 3-body processes and as a function of the masses of the involved particles. In all cases we take the lightest neutralino $\tilde{\chi}_1^0$ to be the LSP. For each decay mode we fix the corresponding \tilde{t}_1 branching fraction to unity; the search is in all other respects designed to be as independent as possible of the details of any specific SUSY model. We explore a range of signal mass points for each decay mode under consideration. In the decay mode tt, the unknown masses are those of the \tilde{t}_1 and the $\tilde{\chi}_1^0$, while in the case of bbWW, a third unknown is the mass of the lightest chargino ($\tilde{\chi}_1^\pm$). In the latter case we consider three possible mass assignments, labeled by the parameter $x = 0.25, 0.50, 0.75$; x is defined by

$$m(\tilde{\chi}_1^\pm) = m(\tilde{\chi}_1^0) + x[m(\tilde{t}_1) - m(\tilde{\chi}_1^0)]. \quad (1)$$

In this paper we expand the result of our previous search in the single-lepton final state [12] by improving key aspects of the signal selection. Since the SM background dominates the signal by several orders of magnitude and often has similar distributions for individual discriminating variables, a multivariate approach has been developed to exploit differences in the correlations among discriminating variables for signal and SM background. The background determination method has also been improved compared to Ref. [12] in order to better control and correct the tail of the key transverse mass distribution. In addition to the single lepton search, we also report on a search in the dilepton mode, where the key discriminating variable is an M_{T2} variable [13]. The final result is based on a combination of the single lepton and dilepton searches.

Table 1: Kinematic conditions for the \tilde{t}_1 decay modes explored in this paper.

Kinematic conditions	Type of decay	Decay mode
$m(b) + m(W) + m(\tilde{\chi}_1^0) \leq m(\tilde{t}_1)$ and $m(\tilde{t}_1) < m(t) + m(\tilde{\chi}_1^0)$	3-body decays (tt)	$\tilde{t}_1 (\rightarrow t^* \tilde{\chi}_1^0) \rightarrow bW\tilde{\chi}_1^0$
$m(t) + m(\tilde{\chi}_1^0) \leq m(\tilde{t}_1)$	2-body decays (tt)	$\tilde{t}_1 \rightarrow t\tilde{\chi}_1^0$, with $t \rightarrow bW$
$m(b) + m(W) + m(\tilde{\chi}_1^0) \leq m(\tilde{t}_1)$ and $m(\tilde{\chi}_1^0) < m(\tilde{\chi}_1^\pm) < m(\tilde{t}_1) - m(b)$	2-body decays (bbWW)	$\tilde{t}_1 \rightarrow b\tilde{\chi}_1^\pm$, with $\tilde{\chi}_1^\pm \rightarrow W^{(*)}\tilde{\chi}_1^0$

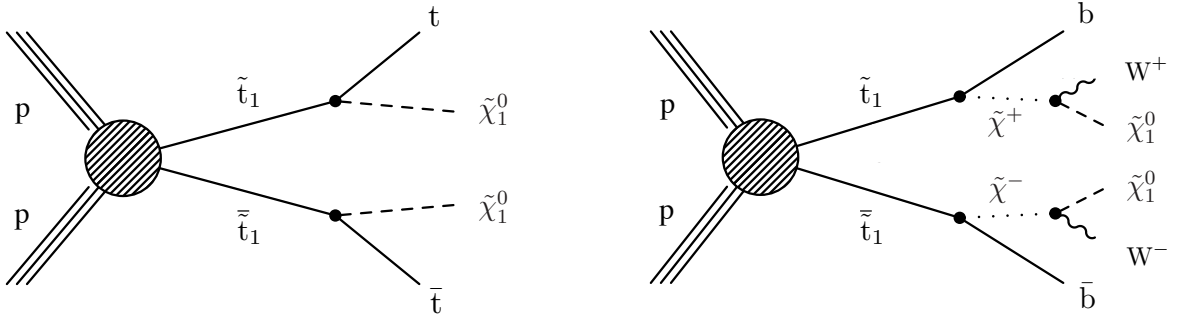


Figure 1: Top squark direct pair production at the LHC. Left: tt decay mode. Right: bbWW decay mode.

2 The CMS detector

The central feature of the CMS apparatus is a superconducting solenoid that provides an axial magnetic field of 3.8 T for charged-particle tracking. Trajectories of charged particles are measured by a silicon pixel and strip tracker, covering $0 < \phi < 2\pi$ in azimuth and $|\eta| < 2.5$, where the pseudorapidity η is defined as $\eta = -\ln[\tan(\theta/2)]$; θ is the polar angle of the trajectory of the particle with respect to the counterclockwise beam direction. A crystal electromagnetic calorimeter and a brass/scintillator hadronic calorimeter surround the tracking detectors. The calorimeter measures the energy and direction of electrons, photons, and hadronic jets. Muons are measured in gas-ionization detectors embedded in the steel flux-return yoke outside the solenoid. The detector is nearly hermetic, allowing for momentum balance measurements in the plane transverse to the beam axis. Events are selected online by a two-level trigger system [14]. A more detailed description of the CMS detector can be found in Ref. [15].

3 Samples, triggers, and reconstruction algorithms

3.1 Samples and trigger requirements

Events used for this search are selected initially by single-lepton and dilepton triggers. For the single-electron final state, the online selection requires the electron be isolated and have transverse momentum $p_T > 27$ GeV; in subsequent offline analysis the reconstructed electron p_T is required to exceed 30 GeV. For the single-muon final state, two triggers are used, which both require $|\eta(\mu)| < 2.1$: a purely leptonic trigger requiring an isolated muon with $p_T > 24$ GeV; and an additional mixed trigger requiring an isolated muon of $p_T > 17$ GeV together with three jets, each having $p_T > 30$ GeV. The first trigger suffices for muons whose offline reconstructed p_T exceeds 26 GeV, while the second trigger allows the analysis to use muons

with reconstructed p_T as low as 20 GeV; the additional jets are required in the analysis in any case. The dilepton triggers require either ee , $\mu\mu$, or $e\mu$ pairs. In each case, one lepton must satisfy $p_T > 17$ GeV and the other lepton must satisfy $p_T > 8$ GeV. Trigger efficiencies are measured in data and applied to simulated events. The integrated luminosity, after data quality requirements, is $19.5 \pm 0.5 \text{ fb}^{-1}$ for the single-lepton states and $19.7 \pm 0.5 \text{ fb}^{-1}$ for the dilepton final states [16].

The SM background processes of relevance to this analysis are $t\bar{t}$, W +jets, $Z/\gamma^* \rightarrow \ell^+\ell^-$ (denoted Drell–Yan, or DY), single top, diboson, triboson, and $t\bar{t} + \text{boson(s)}$. They are simulated by the MADGRAPH [17] (v5.1.3.30) and POWHEG [18] event generators, with CTEQ6L1 [19] and CT10 [20] parton density functions (PDF) respectively. Simulated event samples with signal mass points chosen on a grid of $(m(\tilde{t}_1), m(\tilde{\chi}_1^0))$ values are generated, where the mass of the \tilde{t}_1 varies between 100 and 1000 GeV, and the mass of the $\tilde{\chi}_1^0$ varies between 0 and 700 GeV; as mentioned in Section 1 (see Eq. (1)), three different mass hierarchies are considered for the $bbWW$ decay mode. The generation of signal samples is performed using MADGRAPH with CTEQ6L1 PDF. Parton shower and hadronization are simulated using PYTHIA [21] (v6.4.26 for background and v6.4.22 for signal) with the tune Z2* [22]. All simulated events are propagated through the CMS detector model either with the GEANT4 package [23], or, in the case of the signal samples, with a fast parametric simulation [24]. The next-to-leading-order (NLO) plus the next-to-leading-log (NLL) cross sections for top squark pair production are calculated with PROSPINO [25–30].

To ensure agreement with data, simulated events are weighted so that the distribution of the number of proton-proton interactions per beam crossing agrees with that seen in data; they are additionally weighted by the trigger efficiency and the lepton identification and isolation efficiencies. For simulated $t\bar{t}$ samples, a p_T -dependent weight is applied to match the shape of the $d\sigma(pp \rightarrow t\bar{t} + X)/dp_T$ distribution observed in data. Signal events are weighted to account for the effect of initial state radiation [12].

3.2 Object reconstruction

In this search, all particle candidates are reconstructed with the particle-flow (PF) algorithm [31, 32], and additional criteria are then applied to select electrons, muons, jets, and b jets; the criteria are applied to both collision data and simulation samples.

The identification and measurement of the p_T of muons uses information provided by the silicon detector and the muon system [33]. We require the muon to have a ‘tight’ identification [33] with pseudorapidity $|\eta| < 2.1$ and $|\eta| < 2.4$ for the single-lepton and dilepton searches, respectively. The identification and energy measurement of the electrons uses information provided by the tracker and the electromagnetic calorimeter. Electron candidates are reconstructed in the tracker with the Gaussian-sum filter algorithm [34]. We require the electron to have a ‘medium’ identification [34] with pseudorapidity $|\eta| < 1.44$ and $|\eta| < 2.5$ for the single-lepton and dilepton searches, respectively. Both muon and electron identification demand that the lepton be isolated from the hadronic components of the event. We define an isolation variable for the leptons based on a scalar sum of transverse momenta, $\mathcal{P} \equiv \sum |\vec{p}_T|$, where the sum is taken over all PF candidates within a cone about the lepton of $\Delta R \equiv \sqrt{(\Delta\phi)^2 + (\Delta\eta)^2} = 0.3$, excluding the transverse momentum of the lepton itself, $p_T(\ell)$. In the single-lepton search we impose an upper limit on the absolute isolation, $\mathcal{P} < 5$ GeV; for both searches we impose an upper limit on the relative isolation $\mathcal{P}/p_T(\ell) < 0.15$.

Jets are constructed by clustering all the PF candidates with the anti- k_T jet clustering algorithm [35], using a distance parameter $R = 0.5$. Contamination from additional pp interactions

(pileup) is mitigated by discarding charged PF candidates that are incompatible with having originated from the estimated proton-proton collision point. The average pileup energy associated with neutral hadrons is computed event-by-event and subtracted from the jet energy and from the energy used when computing lepton isolation, i.e., a measure of the activity around the lepton. The energy subtracted is the average pileup energy per unit area (in $\Delta\eta \times \Delta\Phi$) times the jet or isolation cone area [36, 37]. Candidate jets must be separated from selected leptons by $\Delta R > 0.4$. Relative and absolute jet energy corrections are applied to the raw jet momenta to establish a uniform jet response in $|\eta|$ and a calibrated response in jet p_T . We require the jets pass $p_T > 30 \text{ GeV}$ and $|\eta| < 2.4$. To tag jets originating from the hadronization of b quarks, we utilize the combined secondary vertex algorithm at its ‘medium’ operating point [38] with a corresponding efficiency for b jets of 65% and a mistag rate for light jets of 1%. Scale factors are applied to simulation samples to reproduce the efficiencies measured in the data.

As the decays of \tilde{t}_1 are expected to yield neutralinos and neutrinos in their decay chain, genuine missing transverse momentum is expected in the final state of signal events. We define the missing transverse momentum by a sum over the transverse momenta of all PF candidates, $\vec{p}_T^{\text{miss}} \equiv -\sum \vec{p}_T$. All calibration corrections [39] have been applied to candidates used in the sum. The magnitude of the \vec{p}_T^{miss} vector is denoted by $E_T^{\text{miss}} \equiv |\vec{p}_T^{\text{miss}}|$. We reject events where known detector effects or noise lead to anomalously large E_T^{miss} values.

4 Single-lepton search

In the single-lepton search, we consider only final states containing one lepton (e or μ only) and several jets.

4.1 Event Selection

The preselection criteria are defined as follows:

- Exactly one identified and isolated lepton satisfying $p_T(\mu) > 20 \text{ GeV}$ or $p_T(e) > 30 \text{ GeV}$;
- A veto is applied against the presence of a second lepton by requiring that no additional isolated tracks or hadronically decaying τ lepton (τ_h) candidates [12] are present;
- The number of jets and number of b jets must satisfy $N(\text{jets}) \geq 4$ and $N(\text{b jets}) \geq 1$;
- $E_T^{\text{miss}} > 80 \text{ GeV}$;
- $M_T > 100 \text{ GeV}$.

The transverse mass variable is defined by $M_T \equiv \sqrt{2E_T^{\text{miss}} p_T(\ell)(1 - \cos \Delta\phi)}$, where $p_T(\ell)$ is the transverse momentum of the selected lepton and $\Delta\phi$ is the angular difference between the lepton $\vec{p}_T(\ell)$ and \vec{p}_T^{miss} . The requirement on this variable suppresses events in which the source of the lepton and \vec{p}_T^{miss} is W^\pm decay.

At the preselection level, the $t\bar{t}$ and W +jets backgrounds represent 90% and 7%, respectively, of the total expected background (see Section 4.2). For the signal selection, we use a boosted decision tree (BDT) [40] to take advantage of the correlations among variables that discriminate between signal and background; Fig. 2 illustrates how a pair of kinematic variables correlate differently for a background process and signal. Compared to the approach of Ref. [12], the signal selection is characterized mainly by the use of new variables, and a systematic search for the most reduced set of best-performing variables to be used as input to the BDT. Furthermore, because the discriminating power of each input varies across the $(m(\tilde{t}_1), m(\tilde{\chi}_1^0))$ mass plane,

the latter is partitioned and a unique BDT is trained in each partition. The full list of variables (not all used in every BDT) is given below:

- E_T^{miss} : The presence of missing transverse momentum signals the possible production of a stable unseen object, such as the $\tilde{\chi}_1^0$.
- $p_T(\ell)$: The correlation between the missing transverse momentum E_T^{miss} and the lepton transverse momentum $p_T(\ell)$ differs between signal, where genuine E_T^{miss} is due to two missing objects ($\tilde{\chi}_1^0$), and $t\bar{t}$ and W +jets backgrounds where the E_T^{miss} is due to a single missing object (ν).
- $N(\text{jets}), p_T(j_1), p_T(b_1)$: These describe the multiplicity of selected jets and the p_T of the highest p_T jet and highest p_T b jet, respectively.
- M_{T2}^W : The distribution of this variable shows an edge at the top quark mass for $t\bar{t}$ events where both W bosons decay leptonically and one of the leptons is lost.

It is defined by minimizing the following over possible momentum vectors \vec{p}_{T1} and \vec{p}_{T2} :

$$M_{T2}^W = \min \left\{ M_x \text{ consistent with: } \left[\begin{array}{l} \vec{p}_{T1} + \vec{p}_{T2} = \vec{p}_T^{\text{miss}}, \quad (p_1 + p_\ell)^2 \equiv p_2^2 = m(W)^2, \\ p_1^2 = 0, \quad (p_1 + p_\ell + p_{b1})^2 = (p_2 + p_{b2})^2 = M_x^2 \end{array} \right] \right\}. \quad (2)$$

Here p_1 is the momentum of the neutrino associated with a successfully reconstructed lepton in one $W \rightarrow \ell\nu$ decay, and p_2 corresponds to an unreconstructed W whose two decay products (the lost lepton and the neutrino) escape detection. The momenta p_{b1} and p_{b2} are of the b jets with the highest (leading) and second-highest (sub-leading) p_T values, respectively. Including M_{T2}^W in the BDT reduces the contribution of the $t\bar{t}$ dilepton background.

- H_T : The scalar sum $H_T \equiv \sum |\vec{p}_T|$, summed over all jets with $p_T > 30 \text{ GeV}$, characterizes the hadronic component of the event. A related variable H_T^{frac} is defined by $H_T^{\text{frac}} \equiv \sum' |\vec{p}_T| / H_T$, where the terms in the numerator are restricted to jets of $p_T > 30 \text{ GeV}$ that lie in the same hemisphere as \vec{p}_T^{miss} .
- $\Delta R(\ell, b_1), \Delta\phi(j_{1,2}, \vec{p}_T^{\text{miss}})$: Two topological variables, $\Delta R(\ell, b_1)$ and $\Delta\phi(j_{1,2}, \vec{p}_T^{\text{miss}})$, are defined as follows: ΔR is the distance between the lepton and the leading b jet; and $\Delta\phi$ is the minimal angular difference between the \vec{p}_T^{miss} vector and either the leading or sub-leading jet.
- χ_{had}^2 : To characterize the kinematics of $t\bar{t}$ events we build a χ^2 variable comparing the invariant masses of the three- and two-jet systems to the mass of the top quark and W boson, respectively. It is defined as:

$$\chi_{\text{had}}^2 = \frac{(M_{j1j2j3} - m(t))^2}{\sigma_{j1j2j3}^2} + \frac{(M_{j1j2} - m(W))^2}{\sigma_{j1j2}^2}, \quad (3)$$

where M_{j1j2j3} and M_{j1j2} are, respectively the invariant mass of the three-jet system from the top quark and of the two jets posited to originate from W boson decay; σ_{j1j2j3} and σ_{j1j2} are the uncertainties of these invariant masses. The M_{j1j2j3} value is calculated after imposing a $M_{j1j2} = m(W)$ constraint by kinematic fit, while M_{j1j2} is the two-jet invariant mass before the fit. The jet assignments are made according to the b tag information: j3 must be tagged as a b quark if there are at least two b jets in the event, and j1 and j2 cannot be tagged unless there are at least three b jets in the event. This variable is used for the signal selection in the $t\bar{t}$ decay mode.

- $M(3\text{jet})$, $M(\ell b)$: Finally, to kinematically disentangle the signal from the $t\bar{t}$ background, we construct two new invariant-mass variables that characterize the process where one \tilde{t}_1 decays into 3 jets and $\tilde{\chi}_1^0$ while the other decays into a b quark, lepton, neutrino, and $\tilde{\chi}_1^0$. In the case of the bbWW decay mode and the tt decay mode where no on-shell top quark is produced, i.e. $m(\tilde{t}_1) - m(\tilde{\chi}_1^0) < m(t)$, the $M(\ell b)$ distribution discriminates between $t\bar{t}$ and signal. The quantity $M(3\text{jet})$ is the invariant mass of the 3 jets among the 4 highest p_T jets which are the most back-to-back (according to angular difference) to the lepton. In the case of $t\bar{t}$ background, $M(3\text{jet})$ reconstructs the mass of the top quark having decayed into 3 jets, modulo the limitations of the jet association. For the bbWW decay mode of the signal, it reconstructs an invariant mass different from $m(t)$, as no top quark is present in the final state. The quantity $M(\ell b)$ is defined as the invariant mass of the lepton and the b jet closest to it in ΔR .

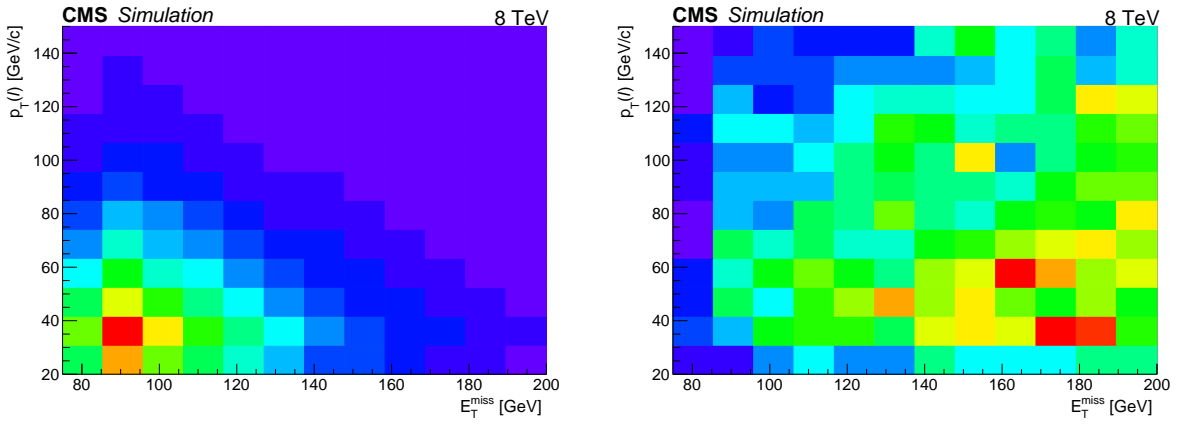


Figure 2: Distribution of the transverse momentum of the lepton versus the missing transverse energy at the preselection, for the simulated $t\bar{t}$ background (left) and for the bbWW decay mode ($x = 0.50$) of the signal with $m(\tilde{t}_1) - m(\tilde{\chi}_1^0) \geq 625$ GeV (right).

Distributions of some of the variables used for the bbWW ($x = 0.75$) decay mode are illustrated in Fig. 3. The figure shows the distributions for both $t\bar{t}$ and signal samples; in the latter case four different kinematic possibilities are illustrated, distinguished by values of Δm :

$$\Delta m \equiv m(\tilde{t}_1) - m(\tilde{\chi}_1^0). \quad (4)$$

The figure shows clearly the evolution of the kinematic distributions as the mass difference between the lightest top squark and the LSP is varied. Differences in kinematic distributions may also be seen when comparing the tt and bbWW signal decay modes, and when varying the choice of x ($x = 0.25, 0.50, 0.75$) in the bbWW decay mode. In Fig. 4 we show distributions of some discriminating variables at the preselection level (but without the restriction on M_T) for both e and μ final states in data and simulated events. The figure shows good agreement between data and the total simulated background, within the uncertainties of the simulated events, which include the statistical uncertainty in the simulation samples quadratically added to the systematic uncertainty in the jet energy scale (JES).

As expected from the distributions shown in Fig. 3, different selection variables will exhibit different degrees of discriminating power, depending on the decay mode (tt or bbWW) and the relevant mass parameters (Δm or x) of the signal. To find the most discriminating variables, we test different sets of candidate BDT input variables, maximizing a figure of merit that compares the expected signal yield to the quadratic sum of the statistical and systematic uncertainties in the expected background yield. To keep the selection tool simple, a new variable is incorporated into the set of input variables only if it leads to a substantial increase in the figure of

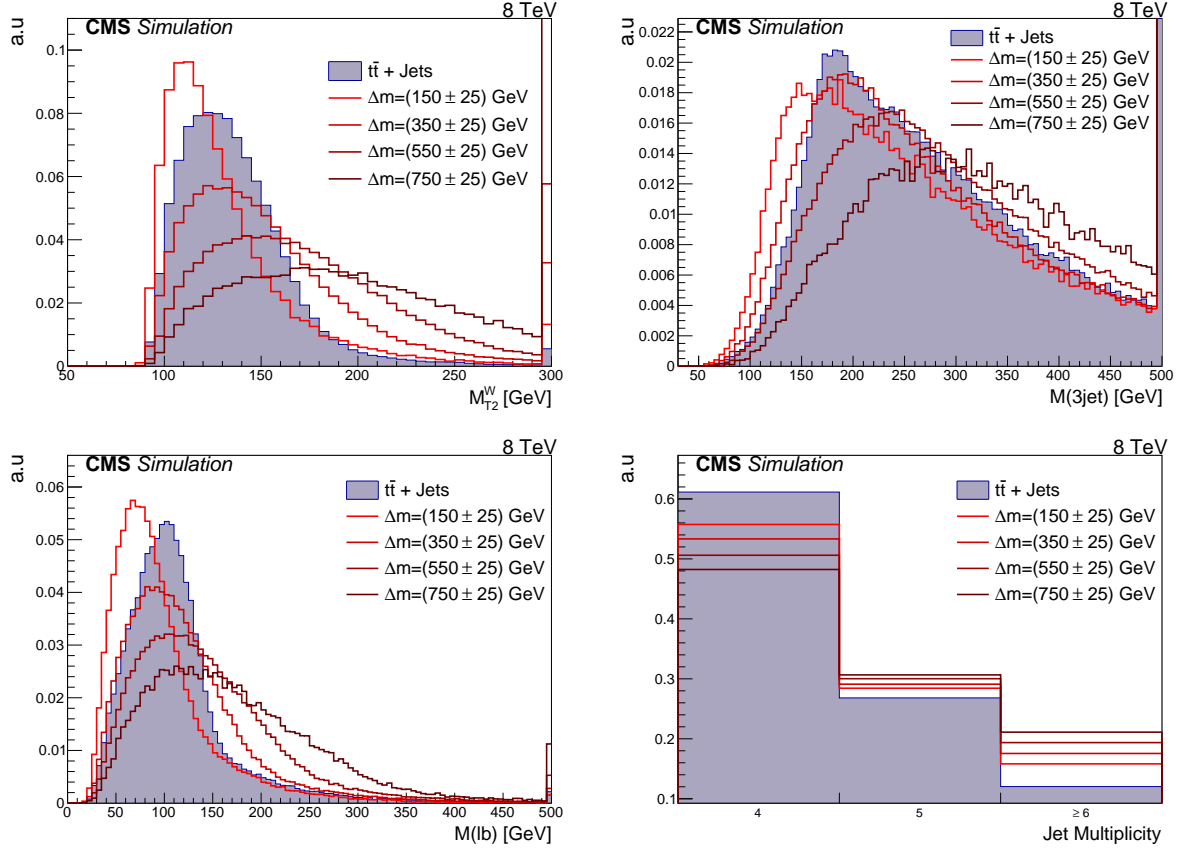


Figure 3: Distribution of some discriminating variables for the $bbWW$ ($x = 0.75$) decay mode at the preselection level, for the main $t\bar{t}$ background and benchmark signal mass points grouped in bands of constant width $\Delta m = (150 \pm 25)$, (350 ± 25) , (550 ± 25) , and (750 ± 25) GeV. Distributions are normalized to the same area. From left to right and from top to bottom: M_{T2}^W , $M(3jet)$, $M(\ell b)$ and $N(jets)$.

merit. The training of the BDT, together with this procedure for selecting variables, is then carried out separately for the different decay modes $t\bar{t}$ and $bbWW$ ($x = 0.25, 0.50, 0.75$), and across six benchmark kinematic regions, defined as: $\Delta m = (150 \pm 25)$, (250 ± 25) , (350 ± 25) , (450 ± 25) , (550 ± 25) , and (650 ± 25) GeV. This partitioning allows us to take into account the evolution of the signal kinematics across the $(m(\tilde{t}_1), m(\tilde{\chi}_1^0))$ plane. The different BDT trainings are numbered from 1 to 6 to reflect the Δm regions in which they are trained.

The final sets of variables retained as input to the BDT are reported in Table 2. Having been chosen with a quantitative assessment of the discriminating power of each variable, these represent the most reduced, while effective, sets of input variables to the BDT, for each decay mode and kinematic region. This represents a new feature of this search compared to Ref. [12], where the BDT was trained with the same set of variables across different kinematic regions. Once the input variables to the BDT are determined, different BDTs are trained in each of the benchmark kinematic regions to build selection tools adapted to a kinematically varying signal. The simulation samples used for finding the best set of variables and training the BDT are statistically independent. This procedure is done for the $t\bar{t}$ and $bbWW$ (different x values) decay modes. Using a more systematic approach for the definition of signal regions (SRs) than in Ref. [12], we first consider which training is the best performing one in the $(m(\tilde{t}_1), m(\tilde{\chi}_1^0))$ plane. We observe that some BDTs are the best over a very limited part of the $(m(\tilde{t}_1), m(\tilde{\chi}_1^0))$ plane, so to

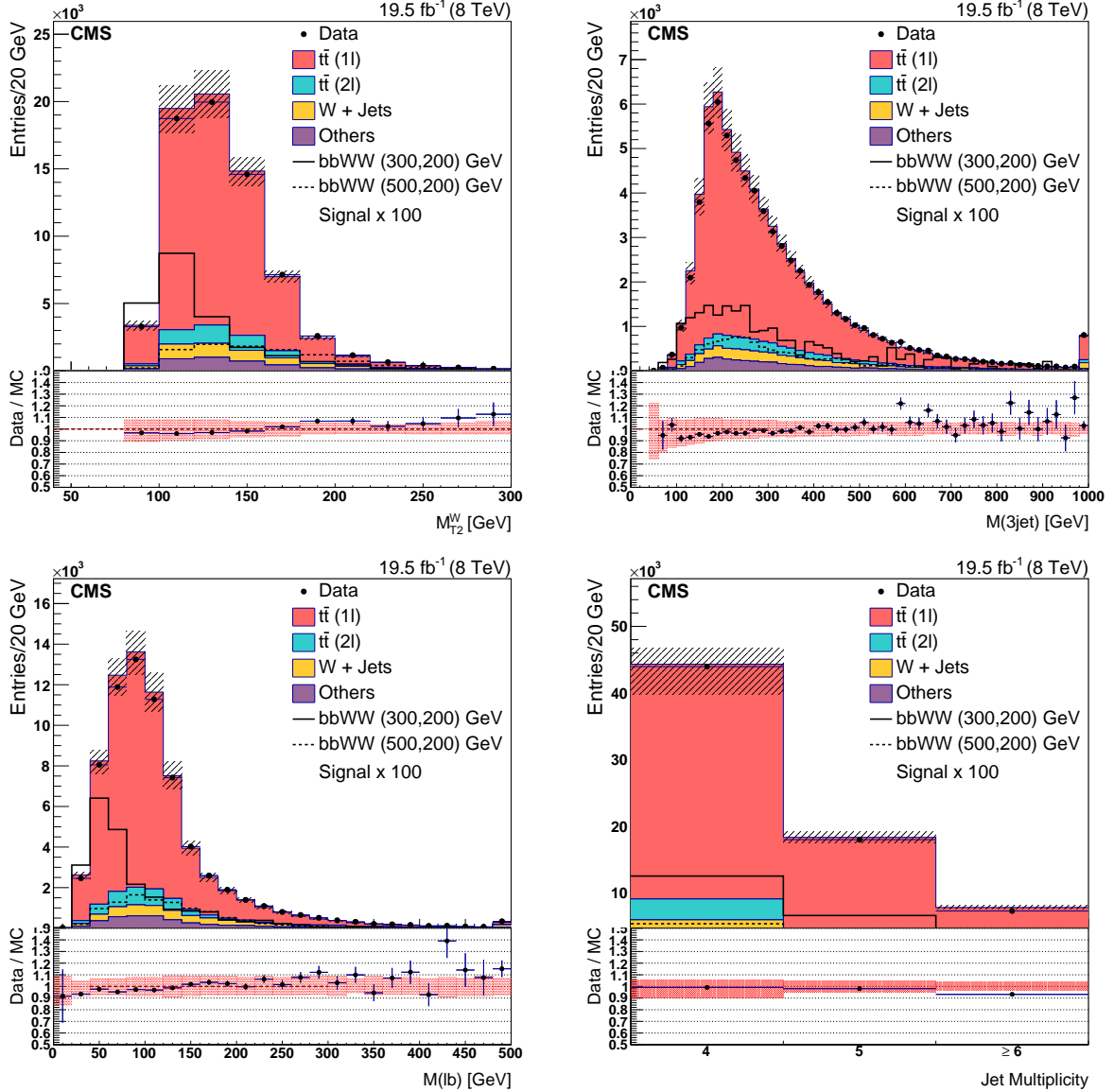


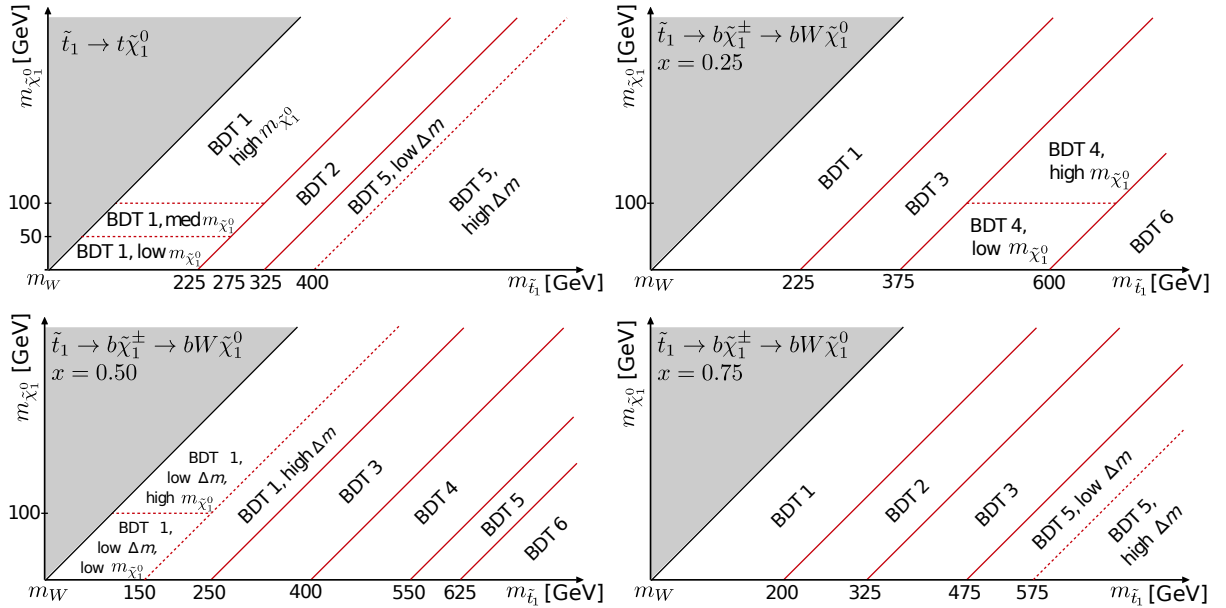
Figure 4: Distributions of different variables in both data and simulation, for both e and μ final states at the preselection level without the M_T requirement. From left to right: M_{T2}^W , $M(3jet)$, $M(\ell b)$ and $N(jets)$. The hatched region represents the quadratic sum of statistical and JES simulation uncertainties. The lower panel shows the ratio of data to total simulation background, with the red band representing the uncertainties mentioned in the text. Two signal mass points of the $bbWW$ decay mode ($x = 0.75$) are represented by open histograms, dashed and solid, with their cross sections scaled by 100; the two mass points $(m(\tilde{t}_1), m(\tilde{\chi}_1^0))$ are (300, 200) and (500, 200) GeV.

simplify the final selection we retain BDT trainings that are observed to be the best performing over a large portion of the mass plane. The resulting SRs, defined as the chosen BDT training in the $(m(\tilde{t}_1), m(\tilde{\chi}_1^0))$ plane, are shown for all considered decay modes in Fig. 5.

With these SRs determined, the final selection is made by applying a minimum threshold to each BDT output as shown in Fig. 6. The thresholds are determined by minimizing the expected upper limit cross section (σ_{95}^{exp}) obtained from events remaining above the threshold, taking into account the predicted background (Section 4.2). The final BDT trainings and selections are

Table 2: Final selection variables chosen as input for the BDT training, as functions of the decay modes bbWW and tt, and kinematic regions. Column headings ΔR and $\Delta\phi$ refer to $\Delta R(\ell, b_1)$ and $\Delta\phi(j_{1,2}, \vec{p}_T^{\text{miss}})$.

	E_T^{miss}	$p_T(\ell)$	M_{T2}^W	$N(\text{jets})$	$p_T(j_1)$	$p_T(b_1)$	H_T	H_T^{frac}	ΔR	$\Delta\phi$	χ_{had}^2	$M(\ell b)$	$M(3\text{jet})$
tt:													
$\Delta m < m(t)$	✓	✓		✓		✓		✓		✓		✓	
$\Delta m \geq m(t)$	✓	✓	✓	✓	✓			✓	✓	✓	✓		
bbWW:													
$x = 0.25, 0.50$	✓	✓	✓	✓		✓			✓	✓		✓	✓
$x = 0.75$	✓	✓	✓	✓	✓		✓			✓		✓	✓



reported in Fig. 5 for all decay modes; within some SRs, the same BDT training is used with different threshold values, thus leading to different selections. On average the BDT selection suppresses the SM background by a factor $\sim 10^3$ while reducing the signal only by a factor ~ 10 ; the performance improves monotonically with increasing Δm .

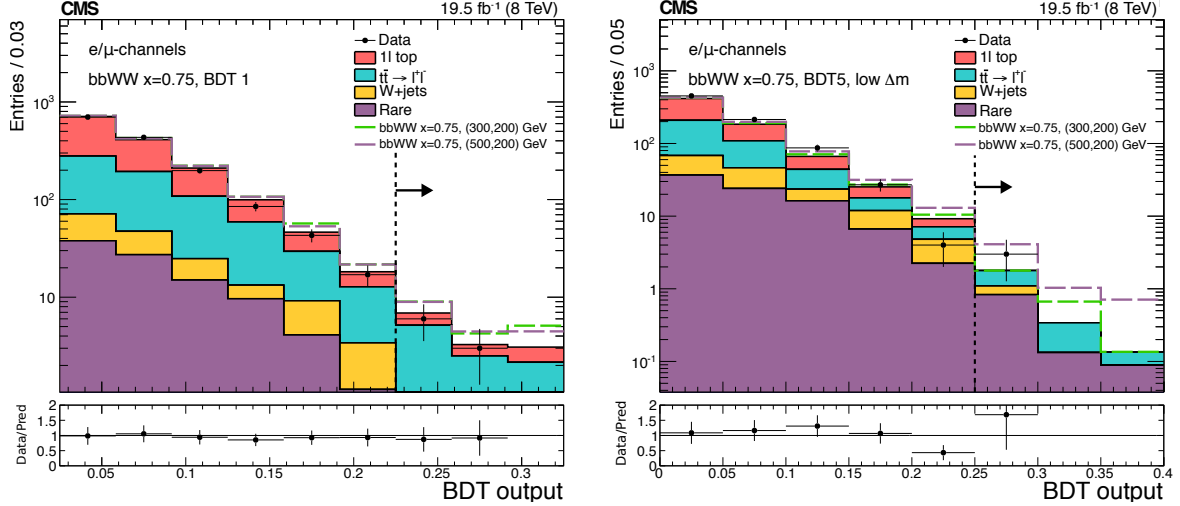


Figure 6: The BDT output distributions of the $bbWW$ ($x = 0.75$) decay mode in both final states at the preselection level for data and predicted background, with $BDT1 > 0.025$ (left) and $BDT5 > 0$ (right). Two representative signal mass points are shown: $(m(\tilde{t}_1), m(\tilde{\chi}_1^0)) = (300, 200)$ and $(500, 200)$ GeV. In each panel the final selection is indicated by the vertical black dashed line. The normalization and M_T correction (see Section 4.2.2), computed in the tail of the BDT output, i.e. to the right of the dashed line, are here propagated to the full distribution. The uncertainties are statistical. The plots on the bottom represent the ratio of Data over the predicted background, where we quadratically add statistical uncertainties with the uncertainties on the scale factors.

4.2 Background estimation

The SM background processes in the single-lepton search can be divided into four categories. At preselection, the dominant contribution ($\sim 66\%$ of the total) is the $t\bar{t}$ production with one lepton; we include single top-quark production in this category and call the combination the “ $t\bar{t} \rightarrow 1\ell$ ” component. The second most significant background (23%) comes from $t\bar{t}$ events with two leptons, where one lepton escapes detection; we will call this the “ $t\bar{t} \rightarrow \ell\ell$ ” component. The third background (7%) is the production of W in association with jets, which we will denote “ W +jets”. Other backgrounds are labeled as “rare”. We use data to estimate the event yields of the first three categories, starting with distributions obtained from simulation, and normalizing these with scale factors (SF) determined in control regions. The background is estimated using the formulae:

$$\begin{aligned} N_{\text{tail}}(t\bar{t} \rightarrow 1\ell) &= SF_0 N_{\text{tail}}^{\text{MC}}(t\bar{t} \rightarrow 1\ell) SFR_{1\ell}, \\ N_{\text{tail}}(t\bar{t} \rightarrow \ell\ell) &= SF_{\ell\ell} N_{\text{tail}}^{\text{MC}}(t\bar{t} \rightarrow \ell\ell), \\ N_{\text{tail}}(W\text{+jets}) &= SF_0 N_{\text{tail}}^{\text{MC}}(W\text{+jets}) SFR_W. \end{aligned} \quad (5)$$

The subscript *tail* refers to the region $M_T > 100$ GeV. The simulation yields at the final selection level ($N_{\text{tail}}^{\text{MC}}$) are corrected by normalization scale factors $SF_{\ell\ell}$ and SF_0 (defined in Eq. (6) and (7)), determined in the M_T peak region $50 < M_T < 80$ GeV. The additional scale factor ratios, denoted $SFR_{1\ell}$ and SFR_W , are used to correct the tail of the M_T distribution, and are determined

using a control region with zero b jets. The procedure accounts for the possibility of signal contamination in the different control regions. At the final selection level the $t\bar{t} \rightarrow \ell\ell$ process represents an approximately constant proportion of the total background at $\sim 60\%$, while the $t\bar{t} \rightarrow 1\ell$ and W +jets processes have varying proportions across the different selections within the remaining $\sim 40\%$. Signal contamination is important only at low Δm , where it alters the background determination by up to 25%.

4.2.1 Normalization in the M_T peak

The scale factors $SF_{\ell\ell}$ and SF_0 are estimated to correct for the normalization in the M_T peak region and after the final selection on the output of the BDT. To calculate SF_0 we further require the second lepton veto, while $SF_{\ell\ell}$ is obtained without this veto. $SF_{\ell\ell}$ fixes the $t\bar{t} \rightarrow \ell\ell$ background normalization, while SF_0 sets the $t\bar{t} \rightarrow 1\ell$ and W +jets background normalizations. The scale factors are computed as follows:

$$SF_{\ell\ell} = \left(\frac{N(\text{data}) - N^{\text{MC}}(\text{rare}) - N^{\text{MC}}(\text{signal})}{N^{\text{MC}}(t\bar{t} \rightarrow 1\ell) + N^{\text{MC}}(t\bar{t} \rightarrow \ell\ell) + N^{\text{MC}}(W+\text{jets})} \right), \quad (6)$$

$$SF_0 = \left(\frac{N(\text{data}) - N^{\text{MC}}(\text{rare}) - N^{\text{MC}}(\text{signal}) - SF_{\ell\ell} N^{\text{MC}}(t\bar{t} \rightarrow \ell\ell)}{N^{\text{MC}}(t\bar{t} \rightarrow 1\ell) + N^{\text{MC}}(W+\text{jets})} \right). \quad (7)$$

The inclusion of the $N^{\text{MC}}(\text{signal})$ term accounts for possible signal contamination. At preselection we have: $SF_{\ell\ell} = (1.06 \pm 0.01)$ and $SF_0 = (1.05 \pm 0.01)$. At the final selection level, the deviation of these scale factors from unity is always within 10%.

4.2.2 Correction for the tail in the M_T distribution

To study the tail of the M_T distribution for different backgrounds, we enrich the data with the W +jets contribution by inverting the b-tagging criterion of the preselection. The left plot of Fig. 7 compares the data with background simulation, and shows some disagreement between the two for $M_T > 100$ GeV. To correct this, we follow an approach based on template fits, which allows us to extract different correction factors for the $t\bar{t} \rightarrow 1\ell$ and the W +jets backgrounds, rather than assuming them to be equal as in Ref. [12].

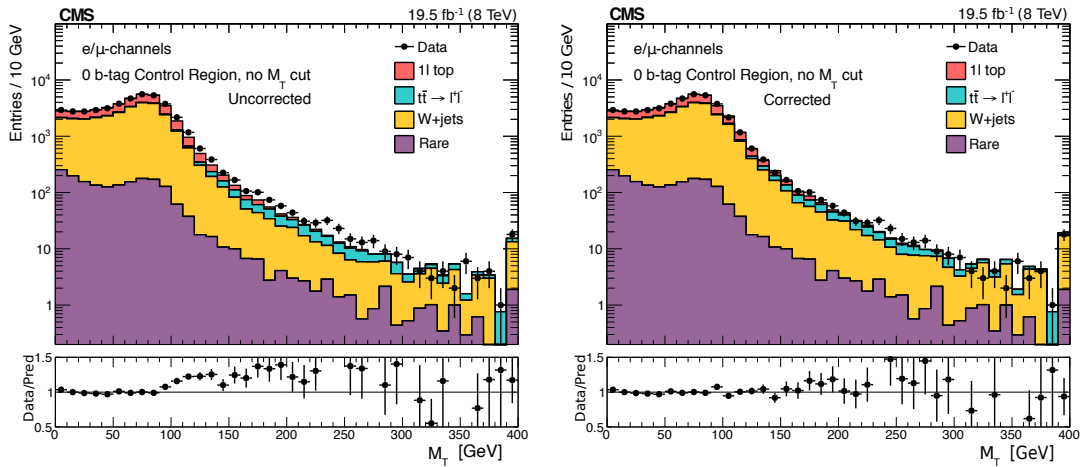


Figure 7: Full M_T distribution in the control region with zero b jets, without any extra signal selection. Left: without the tail correction factors applied; right: with SFR_W and $SFR_{1\ell}$ corrections applied. The plots on the bottom represent the ratio of Data over the predicted background.

The template fit is performed using the invariant mass of the lepton and the jet with the highest b-tag discriminator. This variable, $M'_{\ell b}$, is well modeled by the background simulation (see Fig. 8, left) and exhibits discriminating power between W +jets and $t\bar{t} \rightarrow 1\ell$ (Fig. 8, right). The contributions of the $t\bar{t} \rightarrow \ell\ell$ background, the rare backgrounds, and the signal, are taken from simulation and their normalizations are constrained within a 20% uncertainty during the template fit. The normalizations of the $t\bar{t} \rightarrow 1\ell$ and W +jets backgrounds are free parameters expressed in terms of scale factors SF . The fit is performed in a control region with zero b-tag jets, in two separate regions of the M_T distribution: the peak defined by $50 < M_T < 80$ GeV, and the tail defined by $M_T > 100$ GeV. We then extract the normalization independent ratios $SFR = SF_{\text{tail}}/SF_{\text{peak}}$ for $t\bar{t} \rightarrow 1\ell$ and for W +jets. Without any BDT signal selection and for a case of negligible signal contamination, the fit yields: $SFR_{t\bar{t} \rightarrow 1\ell} = (1.04 \pm 0.16)$ and $SFR_W = (1.33 \pm 0.10)$. The right plot of Fig. 7 confirms the effectiveness of this correction.

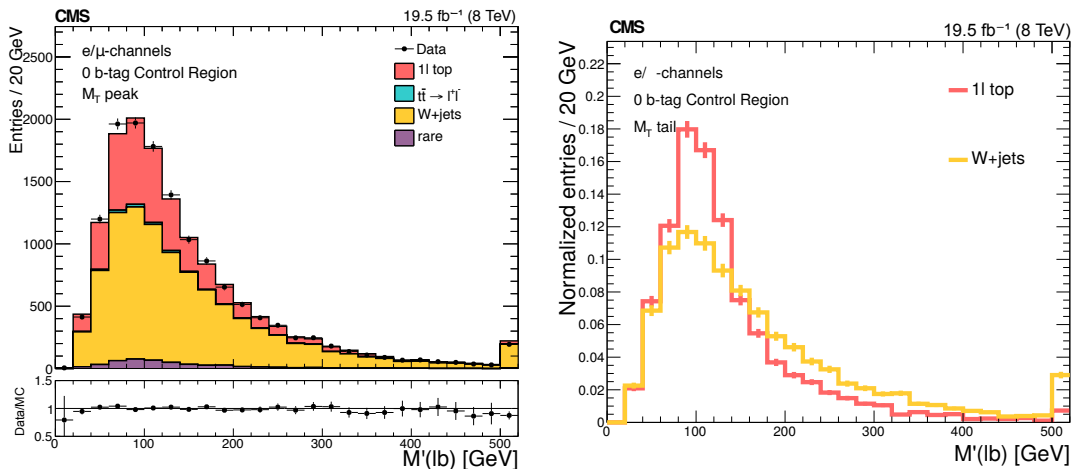


Figure 8: Left: Comparison of data and simulation in the $M'_{\ell b}$ distributions for events with $50 < M_T < 80$ GeV and zero b jets. Right: Shape comparison between $t\bar{t} \rightarrow 1\ell$ and W +jets for $M_T > 100$ GeV.

Due to the low yields after the final selections, we loosen the requirements on the output of the BDT to keep 25% of the total yield when we extract the SFR values. The SFR ratios obtained for the different signal regions within a given decay mode ($t\bar{t}$ or $b\bar{b}WW$) agree well with each other. We therefore set the final SFR factor for each decay mode to the average over the signal regions for that mode. The resulting SFR values for the $t\bar{t}$ and $b\bar{b}WW$ decay modes differ from one another, and also vary across the $(m(\tilde{t}_1), m(\tilde{\chi}_1^0))$ mass plane: $SFR_{1\ell}$ increases from 1.0 to 1.4 with increasing top squark mass, while SFR_W is stable around a mean value ~ 1.2 everywhere. In addition to the extraction of tail correction factors, we check in the control region with zero b jets that the distributions of all input variables in data are well described by the predicted background.

4.3 Systematic uncertainties

The sensitivity of this search is limited by uncertainties in both the background prediction and the acceptance and efficiency of the signal at the mass points under consideration. The uncertainties are listed below.

4.3.1 Background

For systematic uncertainties affecting the predicted background:

- We study the impact of limited simulation statistics, generator scale variations, and JES uncertainty in the template fit method in the control region with zero b jets and no BDT selection. This leads to a global absolute uncertainty of 0.6 in $SFR_{1\ell}$ and 0.4 in SFR_W .
- The goodness of the $t\bar{t} \rightarrow \ell\ell$ background modeling is checked in two different control regions. The first uses events with exactly two leptons in the final state and a lower jet multiplicity ($N(\text{jets}) \geq 2$) than that employed in the preselection; the second uses events with exactly one lepton, and an isolated track or τ_h candidate. The simulation prediction is compared with data in the M_T tail region of these control regions for each BDT selection. The comparison shows overall agreement and deviations are used to derive a relative systematic uncertainty, ranging from 20 to 80% depending on the selection.
- We check the modeling of the $N(\text{jets})$ distribution in the $t\bar{t}$ background with a control region defined to have exactly two leptons and no requirement on M_T . The data/simulation scale factors are observed to be compatible with unity; therefore, no correction factor is used, but the deviations from unity are taken as systematic uncertainty. This leads to a flat 2% uncertainty, used for all the BDT selections.
- A 6% uncertainty for the modeling of the isolated track veto is applied to the fraction of $t\bar{t}$ dilepton background events that have a second e/μ or a one-prong τ_h decay in the acceptance. A 7% uncertainty for the modeling of the hadronic τ veto is only applied to the fraction of $t\bar{t}$ dilepton background events that have a τ_h in the acceptance.
- The $SF_{\ell\ell}$ and SF_0 normalization factors are varied within their statistical uncertainties and the variations are propagated as systematic uncertainties to the M_T peak regions.
- The statistical uncertainties in the simulation background samples are propagated to the systematic uncertainties in the backgrounds.
- The cross section of W +jets and rare backgrounds are conservatively varied by 50%, affecting the prediction of other background processes through $SF_{\ell\ell}$ and SF_0 (see equations of Section 4.2); the cross section of the $t\bar{t}$ process is varied by 10%.

Table 3 gives a summary of the relative systematic uncertainties in the predicted total background yield at the preselection level, as well as their range of variation over the different top squark decay modes and BDT selections.

Table 3: Summary of the relative systematic uncertainties in the total background, at the preselection level, and the range of variation over the BDT selections.

Source	Uncertainty (%) at preselection	Uncertainty (%) range over BDT selections
$SFR_{1\ell}$ uncertainty	16.4	0—24
SFR_W uncertainty	1.4	0—5
Modeling of M_T tail in $t\bar{t} \rightarrow \ell\ell$	1.6	7—39
Modeling of $N(\text{jets})$ in $t\bar{t}$	1.1	1—4
Modeling of the 2 nd lepton veto	1.2	1—4
Normalization in M_T peak (data & MC stat)	0.7	3—37
Simulation statistics in SR	0.4	3—38
Cross section uncertainties	2.0	4—34
Total	16.8	23—58

4.3.2 Signal

The statistical uncertainties in the signal samples are taken into account. The integrated luminosity is known [16] to a precision of 2.6% and the efficiencies of triggers (Section 3.1) applied to the signal yield are known with a precision of 3%. The efficiencies for the identification and isolation of leptons are observed to be consistent within 5% for data and simulation; we take this difference as an uncertainty. The b-tagging efficiency has been varied within its uncertainties for b, c, and light flavor jets, leading to final yield uncertainties within 3% for all signal mass points. The systematic uncertainty in signal yield that is associated with the JES [41] is obtained by varying the jet energy scale within its uncertainty; the final uncertainties for all signal mass points are within 10%. Systematic uncertainties in the signal efficiency due to PDFs have been calculated [42–44], and are constant at $\sim 5\%$. The effect of the systematic uncertainty due to the modeling of ISR jets by the simulation is studied by deriving data/simulation scale factors that depend on $N(\text{jets})$. The maximum size of these uncertainties varies between 8 and 10% for different decay modes.

4.4 Summary of the single-lepton search

We develop a Δm -dependent signal selection tool with BDTs for the $t\bar{t}$ and $bbWW$ decay modes. For each BDT selection shown in Fig. 5 we provide in Table 4 the predicted background yield (without signal contamination) as well as the number of observed data events for the BDT selections. We do not observe any excess of data events compared to the predicted total background. The background composition varies as function of the different SRs of various decay modes. For the $t\bar{t}$ decay mode, the dominant background is $t\bar{t} \rightarrow \ell\ell$ (50–60% of the total background) across all SRs. For the $bbWW$ $x=0.25$ decay mode, the dominant background is $t\bar{t} \rightarrow 1\ell$ for BDT3, BDT4, BDT6 (40–55%), and $t\bar{t} \rightarrow \ell\ell$ for BDT1 (58%). For the $bbWW$ $x=0.5$ decay mode, the dominant background for BDT1 and BDT6 is $t\bar{t} \rightarrow \ell\ell$ (40–70%), while rare processes dominate for BDT4 and BDT5 ($\sim 80\%$). For BDT3, $t\bar{t} \rightarrow \ell\ell$ and rare processes dominate with an equal proportion ($\sim 33\%$). For the $bbWW$ $x=0.75$ decay mode, $t\bar{t} \rightarrow \ell\ell$ is the dominant background (45–65%) for BDT1 to BDT3, while rare processes dominate for BDT5 (47–61%). In Fig. 6 we show the distribution of the BDT output for data and the predicted background (without signal contamination) for two trainings of the $bbWW$ $x = 0.75$ case.

The signal contamination is taken into account by calculating a new estimation of the background in case of signal contamination (see Eqs. (6) and (7)); this is done separately at each signal mass point in the $(m(\tilde{t}_1), m(\tilde{\chi}_1^0))$ plane, and for each of the signal regions defined in Fig. 5. For the calculation of limits (see Section 6), the number of observed events in data and expected signal remain the same, while the expected background is modified to correct for signal contamination in the control regions. While the effect of this contamination is observed to be almost negligible at high Δm , it can modify the background estimate up to 25% at low Δm .

5 Dilepton search

5.1 Selection

For the three dilepton final states considered in this search ($e\mu$, ee , and $\mu\mu$), we define the preselection as follows:

- At least two oppositely charged leptons.
- For the leading and sub-leading lepton, we require $p_T > 20$ and $p_T > 10$ GeV, respectively.

Table 4: Background prediction without signal contamination and observed data for the BDT selections. The total systematic uncertainties are reported for the predicted background.

tt	BDT 1	BDT 1	BDT 1	BDT 2	BDT 5	BDT 5	
	Low $m(\tilde{\chi}_1^0)$	Medium $m(\tilde{\chi}_1^0)$	High $m(\tilde{\chi}_1^0)$		Low Δm	High Δm	
Background	363 ± 35	46 ± 16	19 ± 7	37 ± 13	6 ± 2	4 ± 2	
Data	286	33	17	33	3	1	
bbWW ($x = 0.25$)	BDT 1	BDT 3	BDT 4	BDT 4	BDT 6		
			Low $m(\tilde{\chi}_1^0)$	High $m(\tilde{\chi}_1^0)$			
Background	42 ± 11	29 ± 7	20 ± 5	5 ± 2	6 ± 3		
Data	27	23	19	5	6		
bbWW ($x = 0.50$)	BDT 1	BDT 1	BDT 1	BDT 3	BDT 4	BDT 5	BDT 6
	Low Δm	Low Δm	High Δm				
	Low $m(\tilde{\chi}_1^0)$	High $m(\tilde{\chi}_1^0)$					
Background	14 ± 5	3 ± 2	91 ± 25	7 ± 2	0.8 ± 0.3	0.7 ± 0.4	3 ± 1
Data	16	1	85	4	1	2	5
bbWW ($x = 0.75$)	BDT 1	BDT 2	BDT 3	BDT 5	BDT 5		
				Low Δm	High Δm		
Background	13 ± 4	23 ± 7	11 ± 3	2 ± 1	0.4 ± 0.2		
Data	9	15	6	3	0		

- For all lepton flavors: $M_{\ell+\ell-} > 20$ GeV.
- If more than two lepton pairs are found that satisfy the above three requirements, the pair with the highest p_T is chosen.
- For ee, $\mu\mu$ channels: $|M_Z - M_{\ell+\ell-}| > 25$ GeV (Z boson veto) and $E_T^{\text{miss}} > 40$ GeV.
- $N(\text{jets}) \geq 2$ and $N(\text{b jets}) \geq 1$.

At the preselection level, $t\bar{t}$ production with two leptons represents $\sim 90\%$ of the total expected background.

In this search we separate the signal from the dileptonic $t\bar{t}$ background by constructing a transverse mass variable $M_{T2}^{\ell\ell}$ as defined in Eq. (8). We begin with the two selected leptons ℓ_1 and ℓ_2 . Under the assumption that the \vec{p}_T^{miss} originates only from two neutrinos, we partition the \vec{p}_T^{miss} into two hypothetical neutrinos with transverse momenta $\vec{p}_{T1}^{\text{miss}}$ and $\vec{p}_{T2}^{\text{miss}}$. We calculate the transverse mass M_T of the pairings of these hypothetical neutrinos with their respective lepton candidates and record the maximum of these two M_T . This process is repeated with other viable partitions of the \vec{p}_T^{miss} until the minimum of these maximal M_T values is reached; this minimum is the $M_{T2}^{\ell\ell}$ for the event [13, 45]:

$$M_{T2}^{\ell\ell} = \min_{\vec{p}_{T1}^{\text{miss}} + \vec{p}_{T2}^{\text{miss}} = \vec{p}_T^{\text{miss}}} \left(\max \left[M_T(\vec{p}_T^{\ell_1}, \vec{p}_{T1}^{\text{miss}}), M_T(\vec{p}_T^{\ell_2}, \vec{p}_{T2}^{\text{miss}}) \right] \right). \quad (8)$$

When constructed in this fashion, $M_{T2}^{\ell\ell}$ has the property that its distribution in $t\bar{t} \rightarrow \ell\ell$ events has a kinematic endpoint at $m(W)$. The presence of additional invisible particles for the signal breaks the assumption that the \vec{p}_T^{miss} arises from only two neutrinos; consequently, $M_{T2}^{\ell\ell}$ in dileptonic top squark events does not necessarily have an endpoint at $m(W)$. The value of $m(W)$ therefore dictates the primary demarcation between the control region $M_{T2}^{\ell\ell} < 80$ GeV, and the general signal region $M_{T2}^{\ell\ell} > 80$ GeV. The left plot of Fig. 9 shows the distribution of $M_{T2}^{\ell\ell}$ at the preselection level, where we observe its discriminating power for two representative signal mass points. The distribution of $M_{T2}^{\ell\ell}$ in top squark events, however, depends upon the signal mass point ($m(\tilde{t}_1), m(\tilde{\chi}_1^0)$), as can be observed on the right plot of Fig. 9.

The optimal threshold on $M_{T2}^{\ell\ell}$ for the final selection is thus dependent on the supersymmetric particle masses: using the background predictions from Section 5.2 for the $M_{T2}^{\ell\ell}$ signal region,

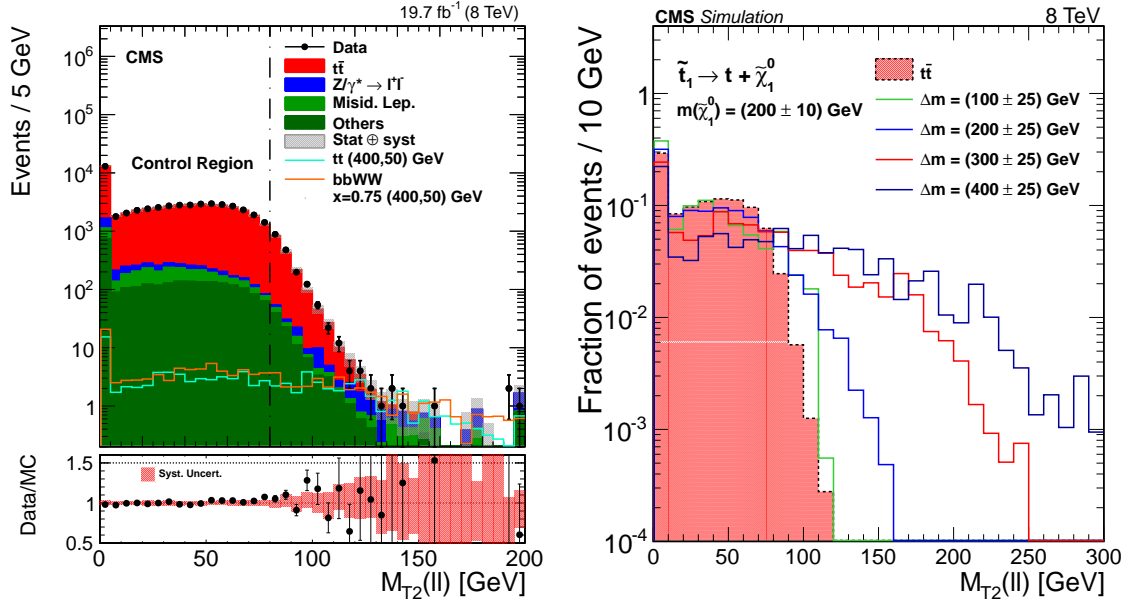


Figure 9: Left: Data, expected background, and signal contributions in the $M_{T2}^{\ell\ell}$ distribution at the preselection level. Background processes are estimated as in Section 5.2. The uncertainty bands are calculated from the full list of uncertainties discussed in Section 5.4. The same signal mass point $(m(\tilde{t}_1), m(\tilde{\chi}_1^0)) = (400, 50)$ GeV is represented for the $t\bar{t}$ and $bbWW$ ($x = 0.75$) decay modes. Right: $M_{T2}^{\ell\ell}$ distribution for the $t\bar{t}$ background and different signal mass points of the $t\bar{t}$ decay mode regrouped in constant Δm bands; distributions are normalized to the same area.

we iterate in 10 GeV steps through possible $M_{T2}^{\ell\ell}$ thresholds, from 80 GeV to 120 GeV; for each $(m(\tilde{t}_1), m(\tilde{\chi}_1^0))$ signal mass point, we pick the threshold that yields the lowest expected upper limit for the top squark production cross section, σ_{95}^{exp} .

5.2 Background prediction

For the $M_{T2}^{\ell\ell}$ signal regions used in this search, the dominant background is $t\bar{t}$. Other backgrounds also contribute, including DY, single-lepton events with an additional misidentified lepton (see Section 5.2.3), and rare processes. The rare processes include single top quarks produced in association with a W boson; diboson production, including W or Z production with an associated photon; triple vector boson production; and $t\bar{t}$ production in association with one or two vector bosons. The normalization of the $t\bar{t}$ and DY backgrounds, and the normalization and shape of the misidentified lepton backgrounds, are evaluated from data using control samples. The shapes of the $t\bar{t}$ and DY backgrounds, and the normalization and shapes of less common processes, are all estimated from the simulation. We perform a number of checks to validate the modeling of the $M_{T2}^{\ell\ell}$ distribution in our simulation (see Section 5.3). For the background processes estimated from simulation, we apply the corrective scale factors mentioned in Sec. 3.2.

5.2.1 $t\bar{t}$ estimation

The $t\bar{t} \rightarrow \ell\ell$ background represents about 90% of the events in the control region $M_{T2}^{\ell\ell} < 80$ GeV (see Fig. 9 left). We can therefore use this region to determine the normalization of the expected SM $t\bar{t}$ contribution in the signal region. To accomplish this, we first count the number of data events in the control region and subtract the simulation background contributions of all non- $t\bar{t}$ backgrounds; we then normalize it by the simulated $t\bar{t}$ yield in the control region. This procedure yields a scale factor of 1.024 ± 0.005 . In this control region, the signal contamination

relative to the expected $t\bar{t}$ contribution depends upon the Δm considered: While being completely negligible at high Δm , it can take values between 5% and 40% at low Δm , depending on Δm as well as the considered top squark decay mode.

5.2.2 Estimation of the Drell–Yan background

To estimate the contribution of DY events in the selected events, we use the Z-boson mass resonance in the $M_{\ell^+\ell^-}$ distribution for opposite charge and same flavor dilepton events. From comparisons with data, we find that our simulation accurately models the Z mass line shape within systematic uncertainties. We can therefore calculate a normalization scale factor for simulated DY events by comparing the observed number of events inside the Z-veto region ($N_{\text{in}}^{\ell^+\ell^-}$) against the expected number of DY events calculated from the simulation ($N_{\text{in}}^{\text{DY}}$),

$$SF_{\text{DY}}^{\ell^+\ell^-} = \frac{\left(N_{\text{in}}^{\ell^+\ell^-} - 0.5N_{\text{in}}^{e\mu}k_{\ell\ell}\right)}{N_{\text{in}}^{\text{DY}}}, \quad (9)$$

where the number of events with different flavor ($N_{\text{in}}^{e\mu}$) is subtracted to account for non-DY processes contaminating $N_{\text{in}}^{\ell^+\ell^-}$. The k -factors in Eq. (9) account for different reconstruction efficiencies for electrons and muons. Using Eq. (9), we calculate a scale factor of (1.43 ± 0.04) for $\mu\mu$ events and (1.46 ± 0.04) for ee events. To account for the contribution of $e\mu$ events originating from $Z \rightarrow \tau^+\tau^-$ decays, we estimate a scale factor of (1.44 ± 0.04) for $e\mu$ events by taking the geometric average of the scale factors for the same-flavor channels.

5.2.3 Misidentified lepton background estimation

The misidentified lepton background consists of events in which non-prompt leptons pass the identification criteria. The largest category of events falling in this group are semileptonic $t\bar{t}$ events and leptonically decaying W events where a jet, or a lepton within a jet, is misreconstructed as an isolated prompt lepton.

In order to have an estimation of this background from data, we first measure the lepton misidentification rate, which is the probability for a non-prompt lepton to pass the requirements of an isolated lepton. This is done by counting the rate at which leptons with relaxed identification (“loose” leptons) pass the “tight” selection requirements (see Section 3.2). The measurement is performed in a data sample dominated by multijet events.

We then measure the prompt lepton rate, which is the efficiency for isolated and prompt leptons to pass selection requirements, in a data sample enriched in $Z \rightarrow \ell^+\ell^-$ events. As with the misidentification rate, the prompt rate is determined by counting the rate at which loose leptons pass tight selection requirements.

Both the measurements of the lepton misidentification rate and the prompt lepton rate are performed as functions of lepton p_T and $|\eta|$. For each dilepton event where both selected leptons pass at least the loose selection requirements, the measured misidentification and prompt rates directly translate into a weight for the event. These weights depend upon whether neither, one, or both loose leptons also passed the tight selection requirements. The shape and normalization of the misidentified lepton background is then extracted by first applying these derived weights to the data sample where both selected leptons pass at least the loose selection requirements, and then calculating the weighted distribution of relevant variables such as $M_{T2}^{\ell\ell}$. Once the background is determined, the number of events falling into the $M_{T2}^{\ell\ell}$ signal regions is found.

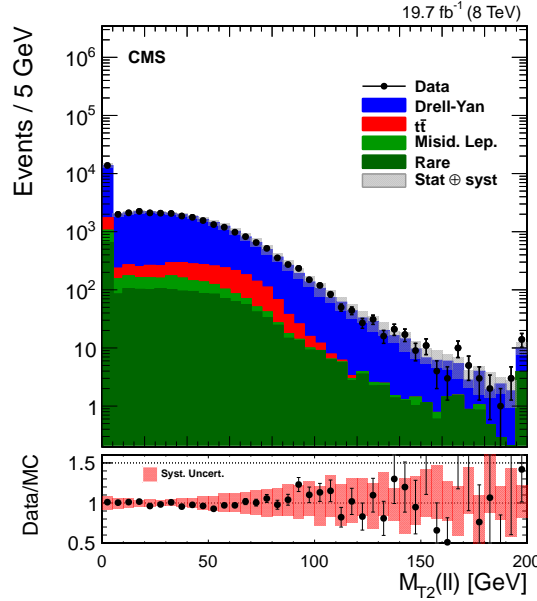


Figure 10: Data and expected background contributions for the $M_{T2}^{\ell\ell}$ distribution in a control region enriched in $Z \rightarrow \ell\ell$ events. This control region is similar to the preselection, except that the Z boson veto and b jet requirements have been inverted. Background processes are estimated as in Section 5.2. The uncertainty bands are calculated from the full list of uncertainties discussed in Section 5.4.

5.3 Checks of the $M_{T2}^{\ell\ell}$ shape

The search in the dileptonic final states requires a good understanding of the $M_{T2}^{\ell\ell}$ shape. In this section we provide a number of validation studies performed with simulation, with comparisons to data in control regions.

One of the main factors determining the $M_{T2}^{\ell\ell}$ shape is the intrinsic resolution and energy scale of the input objects used in the $M_{T2}^{\ell\ell}$ calculation. From studies using $Z \rightarrow \ell\ell$ events, we confirm that the Gaussian core of the E_T^{miss} resolution function is sufficiently well-modeled by the simulation. These studies also confirm that the resolution and scale of the lepton \vec{p}_T are both well-modeled in the simulation.

The intrinsic width of the intermediate W bosons in dileptonic $t\bar{t}$ events drives the shape of the $M_{T2}^{\ell\ell}$ distribution near the kinematic edge at 80 GeV. Comparisons of events with different generated W widths (between 289 MeV and 2.1 GeV) show that any systematic uncertainty in the W boson width has a negligible effect in the selected signal regions.

The final notable effect driving the $M_{T2}^{\ell\ell}$ shape is the category of events populating the tails of the E_T^{miss} resolution function. To confirm that this class of events is modeled in simulation with reasonable accuracy, we perform comparisons between data and simulation in a control region enriched in $Z \rightarrow \ell\ell$ events; this control region is obtained by inverting the Z boson veto and requiring zero reconstructed b jets. Figure 10 shows the $M_{T2}^{\ell\ell}$ distribution in this control region, illustrating that the data distribution, including expected events in the tail, is well-modeled by the simulation.

5.4 Systematic uncertainties

We present the dominant systematic uncertainties affecting the dilepton search.

Table 5: The relevant sources of systematic uncertainty in the background estimate for each signal region used in the limit setting. From left to right, the systematic uncertainty sources are: lepton energy scale (ℓ ES), jet energy scale (JES), unclustered energy scale (Uncl.), E_T^{miss} energy resolution from jets (JER), uncertainty in b tagging scale factors (b tag), lepton selection efficiency (ℓ eff.), ISR reweighting (ISR), the misidentified lepton estimate (ML), and the combined normalization uncertainty in the $t\bar{t}$, DY, and other electroweak backgrounds (σ).

$M_{T2}^{\ell\ell}$	Systematic uncertainties (%)										
	Stat.	ℓ ES	JES	Uncl.	JER	b tag	ℓ eff.	ISR	ML	σ	Total
≥ 80 GeV	± 1	+4 -5	+2 -1	+3 -1	+3 -3	+1 -0	+1 -1	+1 -1	+1 -1	+1 -1	+7 -6
≥ 90 GeV	± 2	+6 -6	+5 -2	+7 -1	+7 -4	+2 -0	+1 -1	+0 -0	+2 -2	+1 -1	+14 -9
≥ 100 GeV	± 4	+6 -5	+9 -2	+10 -1	+12 -2	+1 -1	+1 -1	+2 -1	+3 -3	+2 -2	+20 -9
≥ 110 GeV	± 7	+9 -5	+9 -1	+4 -0	+5 -0	+1 -2	+0 -0	+3 -2	+7 -7	+5 -5	+18 -13
≥ 120 GeV	± 10	+4 -5	+12 -3	+2 -0	+5 -0	+3 -1	+0 -0	+6 -4	+12 -12	+5 -5	+22 -18

5.4.1 Systematic uncertainties affecting the background and signal

The E_T^{miss} measurement, and subsequently the shape of the $M_{T2}^{\ell\ell}$ distribution, is affected by uncertainties in the lepton energy scale, the JES, the jet energy resolution, and the scale of the unclustered energy (objects with $p_T < 10$ GeV) in the event. We vary the four-vector momenta of the lepton and jets within their systematic uncertainties, and propagate the shifted \vec{p}_T back into the E_T^{miss} and $M_{T2}^{\ell\ell}$ calculations. For the jet energy resolution uncertainty, we vary it within its uncertainty and propagate it back into the E_T^{miss} calculation. For the unclustered energy scale, we scale the total \vec{p}_T of the unclustered energy by $\pm 10\%$ and propagate it back into the E_T^{miss} calculation.

As with the single-lepton search (see Section 4.3), we also apply systematic uncertainties to account for the intrinsic statistical uncertainty in the simulation samples as well as any mis-modeling by the simulation of the b-tagging efficiency, the lepton trigger efficiency, the lepton ID and isolation, and the limited modeling of ISR jets by the simulation. No substantial correlation has been observed between the value of $M_{T2}^{\ell\ell}$ and the size of these four systematic uncertainties.

5.4.2 Systematic uncertainties affecting only the background

For the two background normalizations ($t\bar{t}$ and DY), we account for the statistical uncertainty in the normalization. For the misidentified lepton background (see Section 5.2.3), the two primary sources of systematic uncertainty are the statistical uncertainty in the measured rates of prompt and misidentified leptons, and any systematic uncertainty in the measurement of the misidentification rate. Combining these in quadrature yields a total systematic uncertainty of $\sim 75\%$ for the considered signal regions. For the diboson background processes, which are estimated from the simulation, we apply a conservative cross section uncertainty of 50%.

Table 5 displays the magnitude of the effect of the aforementioned systematic uncertainties (Sections 5.4.1 and 5.4.2) on the background estimate for each of the considered signal regions.

5.4.3 Systematic uncertainties affecting only the signal

As in the single-lepton search, we account for the effect of PDF uncertainties in the signal efficiency. The resulting uncertainty in signal efficiency is found to be $\sim 4\%$ across all signal mass points.

5.5 Summary of the dilepton search

We have developed a signal selection based on the $M_{T2}^{\ell\ell}$ distribution. Table 6 presents the predicted backgrounds as well as the number of observed data events for all signal regions; we do not observe any excess of data events compared to the predicted total background. Top quark pair production dominates the composition of the total predicted background in the four signal regions with the lowest $M_{T2}^{\ell\ell}$ threshold, decreasing from 91 % to 45% with increasing threshold, while DY dominates in the last region ($\sim 38\%$). As with the single-lepton search, the signal contamination is also taken into account in the final interpretation of the results.

Table 6: Data yields and background expectation for five different $M_{T2}^{\ell\ell}$ threshold values. The asymmetric uncertainties quoted for the background indicate the total systematic uncertainty, including the statistical uncertainty in the background expectation.

$M_{T2}^{\ell\ell}$ threshold	80 GeV	90 GeV	100 GeV	110 GeV	120 GeV
Data	1785	427	106	30	14
Expected background	1670 $^{+117}_{-104}$	410 $^{+55}_{-35}$	100 $^{+20}_{-8}$	31.8 $^{+5.8}_{-4.0}$	14.8 $^{+3.3}_{-2.7}$

6 Combination and final results

After applying all selections for the single-lepton and dilepton data sets, no evidence for direct top squark production is observed (see Tables 4 and 6). We proceed to combine the results of the two searches. In this combination, no overlap is expected in the event selections of the two searches, and none is observed. Since the background predictions are primarily based on data in the two searches, the corresponding systematic uncertainties are taken to be uncorrelated. Systematic uncertainties affecting the expected signal, as well as those due to luminosity, b tagging, PDF, JES, and lepton identification and isolation, are treated as 100% correlated between the two searches.

We interpret the absence of excess in both single-lepton and dilepton searches in terms of a 95% confidence level (CL) exclusion of top squark pair production in the $(m(\tilde{t}_1), m(\tilde{\chi}_1^0))$ plane. A frequentist CL_s method [46–48] with a one-sided profile is used, taking into account the predicted background and observed number of data events, and the expected signal yield for all signal points. In this method, Poisson likelihoods are assigned to each of the single-lepton and dilepton yields, for each $(m(\tilde{t}_1), m(\tilde{\chi}_1^0))$ signal point, and multiplied to give the combined likelihood for both observations. The final yields of each analysis are taken from the signal region corresponding to the considered signal point. Systematic uncertainties are included as nuisance parameter distributions. A test statistic defined to be the likelihood ratio between the background only and signal plus background hypotheses is used to set exclusion limits on top squark pair production; the distributions of these test statistics are constructed using simulated experiments. When interpreting the results for the tt and bbWW decay modes, we make the hypothesis of unit branching fractions, $\mathcal{B}(\tilde{t}_1 \rightarrow t^{(*)}\tilde{\chi}_1^0) = 1$ and $\mathcal{B}(\tilde{t}_1 \rightarrow b\tilde{\chi}_1^\pm) = 1$, respectively. The expected and observed limits, for which we combine the results of both searches and account for signal contamination, are reported in Fig. 11; the experimental uncertainties are reported on the expected contour, while the PDF uncertainty for the signal cross section,

quadratically added to the systematic uncertainties in $2\mu_r$ and $\mu_r/2$ renormalization scales of the top squark pair production cross section, are reported on the observed contour.

For the $t\bar{t}$ decay mode, we reach sensitivity up to $m(\tilde{t}_1) \sim 700$ GeV for $\tilde{\chi}_1^0$ mass up to ~ 250 GeV; there is a loss of sensitivity along the line $\Delta m = m(t)$, which delineates two different scenarios within the $t\bar{t}$ decay mode (see Table 1) and where the signal acceptance drops dramatically. For the $b\bar{b}WW$ decay mode, the sensitivity reached in this study ranges from 600 to ~ 700 GeV in $m(\tilde{t}_1)$, depending on the values of $m(\tilde{\chi}_1^0)$ and $m(\tilde{\chi}_1^\pm)$; the sensitivity is greater in the case of a large $m(\tilde{\chi}_1^\pm) - m(\tilde{\chi}_1^0)$ mass difference as for $x = 0.75$, where the decay products of the two produced W bosons are more energetic. In the case of $x = 0.50$, there is a drop in sensitivity for $m(\tilde{\chi}_1^\pm) - m(\tilde{\chi}_1^0) \sim m(W)$, which corresponds to the limit in which the W boson is virtual. Because of the rather low threshold achievable in lepton p_T , sensitivity extends down to the kinematic limit $\Delta m \sim m(b) + m(W)$ for the $b\bar{b}WW$ $x = 0.50$ and 0.75 cases.

The final results are dominated by the single-lepton search, where the selection is based on a multivariate selection with new discriminating variables, which is adapted to the kinematics of expected signal events, and where the discriminating power of selection variables is quantitatively assessed. The new signal selection presented in this paper leads to the strengthening and further improvement of the results of Ref. [12]. We now account for systematic uncertainties due to PDFs, and more thoroughly assess the effects of signal contamination. The combination with the dilepton search extends the sensitivity by ~ 25 GeV in the $t\bar{t}$ decay mode in the $\Delta m \gtrsim m(t)$ region, and in the $b\bar{b}WW$ ($x = 0.50$) decay mode across the $m(\tilde{\chi}_1^\pm) - m(\tilde{\chi}_1^0) = m(W)$ region; it very moderately extends the sensitivity in the $b\bar{b}WW$ ($x = 0.75$) at both high \tilde{t}_1 and $\tilde{\chi}_1^0$ masses; no gain of sensitivity is observed in the $b\bar{b}WW$ ($x = 0.25$) case where the search is limited by the small $m(\tilde{\chi}_1^\pm) - m(\tilde{\chi}_1^0)$ mass difference, leaving a rather limited phase space to the decay products of the W boson. The signal contamination (see Section 4.4) reduces the sensitivity of the search by 0–30 GeV depending on the decay mode and signal point under consideration. The limits are rather insensitive to the choice of hypothesis for the polarization of the interaction in the $t\tilde{\chi}_1^0$ and $W\tilde{\chi}_1^0\tilde{\chi}_1^\pm$ couplings for the $t\bar{t}$ and $b\bar{b}WW$ decay modes, respectively.

7 Conclusions

Using up to 19.7 fb^{-1} of pp collision data taken at $\sqrt{s} = 8$ TeV, we search for direct top squark pair production in both single-lepton and dilepton final states. In both searches the standard model background, dominated by the $t\bar{t}$ process, is predicted using control samples in data. In this single-lepton search, we improve the results of Ref. [12] by employing an upgraded multivariate tool for signal selection, fed by both kinematic and topological variables and specifically trained for different decay modes and kinematic regions. This systematic approach to the signal selection, where the discriminating power of each selection variable is quantitatively assessed, is a key feature of the single-lepton search. The background determination method has also been improved compared to Ref. [12]. In the dilepton search the signal selection is based on the $M_{T2}^{\ell\ell}$ variable. In both searches, the effect of the signal contamination is accounted for. No excess above the predicted background is observed in either search. Simplified models (Fig. 1) are used to interpret the results in terms of a region in the $(m(\tilde{t}_1), m(\tilde{\chi}_1^0))$ plane, excluded at 95% CL. We combine the results of both searches for maximal sensitivity; the sensitivity depends on the decay mode, and on the $(m(\tilde{t}_1), m(\tilde{\chi}_1^0))$ signal point. The highest excluded \tilde{t}_1 and $\tilde{\chi}_1^0$ masses are about 700 GeV and 250 GeV, respectively.

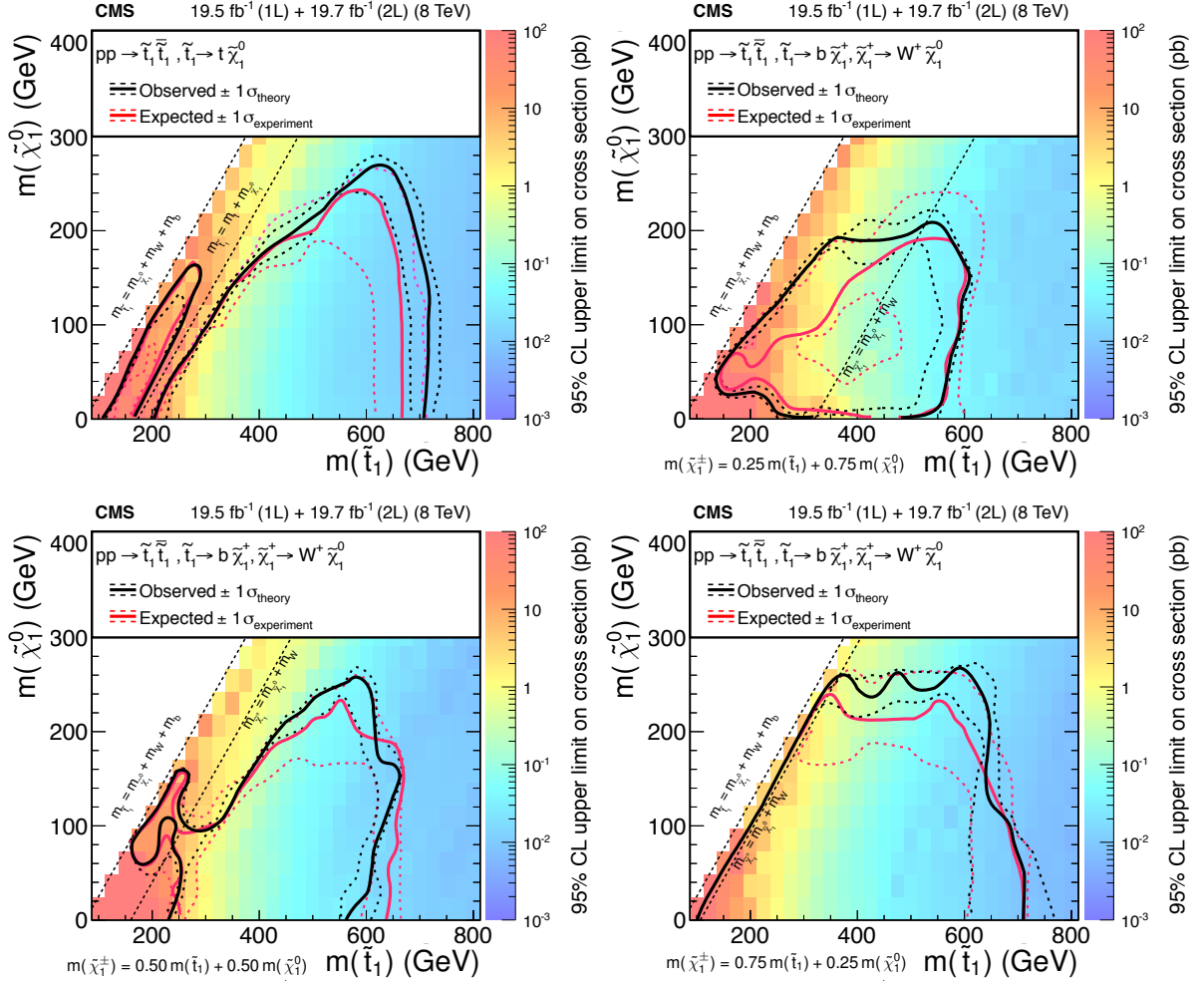


Figure 11: Exclusion limit at 95% CL obtained with a statistical combination of the results from the single-lepton and dilepton searches, for the tt (top left), $bbWW$ $x = 0.25$ (top right), $bbWW$ $x = 0.50$ (bottom left) and $bbWW$ $x = 0.75$ (bottom right) decay modes. The red and black lines represent the expected and observed limits, respectively; the dotted lines represent in each case the $\pm 1\sigma$ variations of the contours. For all decay modes, we show the kinematic limit $m(\tilde{t}_1) = m(b) + m(W) + m(\tilde{\chi}_1^0)$ on the left side of the $(m(\tilde{t}_1), m(\tilde{\chi}_1^0))$ plane; for the tt decay mode, we show the $\Delta m = m(t)$ line; and for the $bbWW$ decay mode, we show the $m(\tilde{\chi}_1^\pm) - m(\tilde{\chi}_1^0) = m(W)$ line.

Acknowledgments

We congratulate our colleagues in the CERN accelerator departments for the excellent performance of the LHC and thank the technical and administrative staffs at CERN and at other CMS institutes for their contributions to the success of the CMS effort. In addition, we gratefully acknowledge the computing centres and personnel of the Worldwide LHC Computing Grid for delivering so effectively the computing infrastructure essential to our analyses. Finally, we acknowledge the enduring support for the construction and operation of the LHC and the CMS detector provided by the following funding agencies: the Austrian Federal Ministry of Science, Research and Economy and the Austrian Science Fund; the Belgian Fonds de la Recherche Scientifique, and Fonds voor Wetenschappelijk Onderzoek; the Brazilian Funding Agencies (CNPq, CAPES, FAPERJ, and FAPESP); the Bulgarian Ministry of Education and Science; CERN; the Chinese Academy of Sciences, Ministry of Science and Technology, and Na-

tional Natural Science Foundation of China; the Colombian Funding Agency (COLCIENCIAS); the Croatian Ministry of Science, Education and Sport, and the Croatian Science Foundation; the Research Promotion Foundation, Cyprus; the Ministry of Education and Research, Estonian Research Council via IUT23-4 and IUT23-6 and European Regional Development Fund, Estonia; the Academy of Finland, Finnish Ministry of Education and Culture, and Helsinki Institute of Physics; the Institut National de Physique Nucléaire et de Physique des Particules / CNRS, and Commissariat à l'Énergie Atomique et aux Énergies Alternatives / CEA, France; the Bundesministerium für Bildung und Forschung, Deutsche Forschungsgemeinschaft, and Helmholtz-Gemeinschaft Deutscher Forschungszentren, Germany; the General Secretariat for Research and Technology, Greece; the National Scientific Research Foundation, and National Innovation Office, Hungary; the Department of Atomic Energy and the Department of Science and Technology, India; the Institute for Studies in Theoretical Physics and Mathematics, Iran; the Science Foundation, Ireland; the Istituto Nazionale di Fisica Nucleare, Italy; the Ministry of Science, ICT and Future Planning, and National Research Foundation (NRF), Republic of Korea; the Lithuanian Academy of Sciences; the Ministry of Education, and University of Malaya (Malaysia); the Mexican Funding Agencies (CINVESTAV, CONACYT, SEP, and UASLP-FAI); the Ministry of Business, Innovation and Employment, New Zealand; the Pakistan Atomic Energy Commission; the Ministry of Science and Higher Education and the National Science Centre, Poland; the Fundação para a Ciência e a Tecnologia, Portugal; JINR, Dubna; the Ministry of Education and Science of the Russian Federation, the Federal Agency of Atomic Energy of the Russian Federation, Russian Academy of Sciences, and the Russian Foundation for Basic Research; the Ministry of Education, Science and Technological Development of Serbia; the Secretaría de Estado de Investigación, Desarrollo e Innovación and Programa Consolider-Ingenio 2010, Spain; the Swiss Funding Agencies (ETH Board, ETH Zurich, PSI, SNF, UniZH, Canton Zurich, and SER); the Ministry of Science and Technology, Taipei; the Thailand Center of Excellence in Physics, the Institute for the Promotion of Teaching Science and Technology of Thailand, Special Task Force for Activating Research and the National Science and Technology Development Agency of Thailand; the Scientific and Technical Research Council of Turkey, and Turkish Atomic Energy Authority; the National Academy of Sciences of Ukraine, and State Fund for Fundamental Researches, Ukraine; the Science and Technology Facilities Council, UK; the US Department of Energy, and the US National Science Foundation.

Individuals have received support from the Marie-Curie programme and the European Research Council and EPLANET (European Union); the Leventis Foundation; the A. P. Sloan Foundation; the Alexander von Humboldt Foundation; the Belgian Federal Science Policy Office; the Fonds pour la Formation à la Recherche dans l'Industrie et dans l'Agriculture (FRIA-Belgium); the Agentschap voor Innovatie door Wetenschap en Technologie (IWT-Belgium); the Agence Nationale de la Recherche ANR-12-JS05-002-01 (France); the Ministry of Education, Youth and Sports (MEYS) of the Czech Republic; the Council of Science and Industrial Research, India; the HOMING PLUS programme of the Foundation for Polish Science, cofinanced from European Union, Regional Development Fund; the OPUS programme of the National Science Center (Poland); the Compagnia di San Paolo (Torino); the Consorzio per la Fisica (Trieste); MIUR project 20108T4XTM (Italy); the Thalís and Aristeia programmes cofinanced by EU-ESF and the Greek NSRF; the National Priorities Research Program by Qatar National Research Fund; the Rachadapisek Sompot Fund for Postdoctoral Fellowship, Chulalongkorn University (Thailand); and the Welch Foundation, contract C-1845.

References

- [1] ATLAS Collaboration, “Observation of a new particle in the search for the Standard Model Higgs boson with the ATLAS detector at the LHC”, *Phys. Lett. B* **716** (2012) 1, doi:10.1016/j.physletb.2012.08.020, arXiv:1207.7214.
- [2] CMS Collaboration, “Observation of a new boson at a mass of 125 GeV with the CMS experiment at the LHC”, *Phys. Lett. B* **716** (2012) 30, doi:10.1016/j.physletb.2012.08.021, arXiv:1207.7235.
- [3] CMS Collaboration, “Combined results of searches for the standard model Higgs boson in pp collisions at $\sqrt{s} = 7$ TeV”, *Phys. Lett. B* **710** (2012) 26, doi:10.1016/j.physletb.2012.02.064, arXiv:1202.1488.
- [4] C. Boehm, A. Djouadi, and M. Drees, “Light scalar top quarks and supersymmetric dark matter”, *Phys. Rev. D* **62** (2000) 035012, doi:10.1103/PhysRevD.62.035012, arXiv:hep-ph/9911496.
- [5] C. Balázs, M. Carena, and C. E. M. Wagner, “Dark matter, light stops and electroweak baryogenesis”, *Phys. Rev. D* **70** (2004) 015007, doi:10.1103/PhysRevD.70.015007, arXiv:hep-ph/403224.
- [6] D0 Collaboration, “Search for 3- and 4-body decays of the scalar top quark in $p\bar{p}$ collisions at $\sqrt{s} = 1.8$ TeV”, *Phys. Lett. B* **581** (2004) 147, doi:10.1016/j.physletb.2003.12.001.
- [7] D0 Collaboration, “Search for pair production of the scalar top quark in muon+tau final states”, *Phys. Lett. B* **710** (2012) 578, doi:10.1016/j.physletb.2012.03.028, arXiv:1202.1978.
- [8] D0 Collaboration, “Search for the lightest scalar top quark in events with two leptons in $p\bar{p}$ collisions at $\sqrt{s} = 1.96$ -TeV”, *Phys. Lett. B* **659** (2008) 500, doi:10.1016/j.physletb.2007.11.086, arXiv:0707.2864.
- [9] CDF Collaboration, “Search for the supersymmetric partner of the top quark in $p\bar{p}$ collisions at $\sqrt{s} = 1.96$ TeV”, *Phys. Rev. D* **82** (2010) 092001, doi:10.1103/PhysRevD.82.092001, arXiv:1009.0266.
- [10] CDF Collaboration, “Search for the supersymmetric partner of the top quark in dilepton events from $p\bar{p}$ collisions at $\sqrt{s} = 1.8$ TeV”, *Phys. Rev. Lett.* **90** (2003) 251801, doi:10.1103/PhysRevLett.90.251801, arXiv:hep-ex/0302009.
- [11] ATLAS Collaboration, “ATLAS Run 1 searches for direct pair production of third-generation squarks at the Large Hadron Collider”, *Eur. Phys. J. C* **75** (2015) 510, doi:10.1140/epjc/s10052-015-3726-9, arXiv:1506.08616.
- [12] CMS Collaboration, “Search for top-squark pair production in the single-lepton final state in pp collisions at $\sqrt{s} = 8$ TeV”, *Eur. Phys. J. C* **73** (2013) 2677, doi:10.1140/epjc/s10052-013-2677-2, arXiv:1308.1586.
- [13] M. Burns, K. Kong, K. T. Matchev, and M. Park, “Using Subsystem MT2 for Complete Mass Determinations in Decay Chains with Missing Energy at Hadron Colliders”, *JHEP* **03** (2009) 143, doi:10.1088/1126-6708/2009/03/143, arXiv:0810.5576.

- [14] CMS Collaboration, “CMS. The TriDAS project. Technical design report, vol. 1: The trigger systems”, LHCC Technical Design Report, CERN-LHCC-2000-038, CERN, 2000.
- [15] CMS Collaboration, “The CMS experiment at the CERN LHC”, *JINST* **3** (2008) S08004, doi:10.1088/1748-0221/3/08/S08004.
- [16] CMS Collaboration, “CMS Luminosity Based on Pixel Cluster Counting – Summer 2013 Update”, CMS Physics Analysis Summary CMS-PAS-LUM-13-001, CERN, 2013.
- [17] J. Alwall et al., “MadGraph 5: going beyond”, *JHEP* **06** (2011) 128, doi:10.1007/JHEP06(2011)128, arXiv:1106.0522.
- [18] S. Frixione, P. Nason, and G. Ridolfi, “A Positive-weight next-to-leading-order Monte Carlo for heavy flavour hadroproduction”, *JHEP* **09** (2007) 126, doi:10.1088/1126-6708/2007/09/126, arXiv:0707.3088.
- [19] J. Pumplin et al., “New generation of parton distributions with uncertainties from global QCD analysis”, *JHEP* **07** (2002) 012, doi:10.1088/1126-6708/2002/07/012, arXiv:hep-ph/0201195.
- [20] H.-L. Lai et al., “New parton distributions for collider physics”, *Phys. Rev. D* **82** (2010) 074024, doi:10.1103/PhysRevD.82.074024, arXiv:1007.2241.
- [21] T. Sjöstrand, S. Mrenna, and P. Skands, “PYTHIA 6.4 physics and manual”, *JHEP* **05** (2006) 026, doi:10.1088/1126-6708/2006/05/026, arXiv:hep-ph/0603175.
- [22] CMS Collaboration, “Study of the underlying event at forward rapidity in pp collisions at $\sqrt{s} = 0.9, 2.76$, and 7 TeV”, *J. High Energy Phys.* **04** (2013) 072, doi:10.1007/JHEP04(2013)072.
- [23] GEANT4 Collaboration, “GEANT4—a simulation toolkit”, *Nucl. Instrum. Meth. A* **506** (2003) 250, doi:10.1016/S0168-9002(03)01368-8.
- [24] S. Abdullin et al., “The fast simulation of the CMS detector at LHC”, in *Intl. Conf. on Computing in High Energy and Nuclear Physics (CHEP 2010)*. 2012. J. Phys.: Conf. Ser. 331 (2012) 032049. doi:10.1088/1742-6596/331/3/032049.
- [25] W. Beenakker, R. Hopker, and M. Spira, “PROSPINO: A Program for the production of supersymmetric particles in next-to-leading order QCD”, (1996). arXiv:hep-ph/9611232.
- [26] W. Beenakker, R. Höpker, M. Spira, and P. M. Zerwas, “Squark and gluino production at hadron colliders”, *Nucl. Phys. B* **492** (1997) 51, doi:10.1016/S0550-3213(97)80027-2, arXiv:hep-ph/9610490.
- [27] A. Kulesza and L. Motyka, “Threshold resummation for squark-antisquark and gluino-pair production at the LHC”, *Phys. Rev. Lett.* **102** (2009) 111802, doi:10.1103/PhysRevLett.102.111802, arXiv:hep-ph/0807.2405.
- [28] A. Kulesza and L. Motyka, “Soft gluon resummation for the production of gluino-gluino and squark-antisquark pairs at the LHC”, *Phys. Rev. D* **80** (2009) 095004, doi:10.1103/PhysRevD.80.095004, arXiv:hep-ph/0905.4749.
- [29] W. Beenakker et al., “Soft-gluon resummation for squark and gluino hadroproduction”, *JHEP* **12** (2009) 41, doi:10.1088/1126-6708/2009/12/041, arXiv:hep-ph/0909.4418.

- [30] W. Beenakker et al., “Squark and gluino production”, *Int. J. Mod. Phys. A* **26** (2011) 2637, doi:10.1142/S0217751X11053560, arXiv:hep-ph/1105.1110.
- [31] CMS Collaboration, “Particle-Flow Event Reconstruction in CMS and Performance for Jets, Taus, and E_T^{miss} ”, CMS Physics Analysis Summary CMS-PAS-PFT-09-001, CERN, 2009.
- [32] CMS Collaboration, “Commissioning of the Particle-flow Event Reconstruction with the first LHC collisions recorded in the CMS detector”, CMS Physics Analysis Summary CMS-PAS-PFT-10-001, CERN, 2010.
- [33] CMS Collaboration, “Performance of CMS muon reconstruction in pp collision events at $\sqrt{s} = 7$ TeV”, *JINST* **7** (2012) P10002, doi:10.1088/1748-0221/7/10/P10002, arXiv:1206.4071.
- [34] CMS Collaboration, “Performance of electron reconstruction and selection with the CMS detector in proton-proton collisions at $\sqrt{s} = 8$ TeV”, *J. Instrum.* **10** (2015) P06005, doi:10.1088/1748-0221/10/06/P06005.
- [35] M. Cacciari, G. P. Salam, and G. Soyez, “The anti- k_t jet clustering algorithm”, *JHEP* **04** (2008) 063, doi:10.1088/1126-6708/2008/04/063, arXiv:0802.1189.
- [36] M. Cacciari and G. P. Salam, “Pileup subtraction using jet area”, *Phys. Lett. B* **659** (2008) 119, doi:10.1016/j.physletb.2007.09.077, arXiv:0707.1378.
- [37] M. Cacciari, G. P. Salam, and G. Soyez, “The catchment area of jets”, *JHEP* **04** (2008) 005, doi:10.1088/1126-6708/2008/04/005, arXiv:0802.1188.
- [38] CMS Collaboration, “Identification of b-quark jets with the CMS experiment”, *JINST* **8** (2013) P04013, doi:10.1088/1748-0221/8/04/P04013, arXiv:1211.4462.
- [39] CMS Collaboration, “Performance of the CMS missing transverse momentum reconstruction in pp data at $\sqrt{s} = 8$ TeV”, *J. Instrum.* **10** (2015) P02006, doi:10.1088/1748-0221/10/02/P02006.
- [40] L. Rokach and O. Maimon, “Data mining with decision trees: theory and applications”. World Scientific Pub Co Inc., 2008. ISBN: 978-981-277-171-1.
- [41] CMS Collaboration, “Determination of jet energy calibration and transverse momentum resolution in CMS”, *JINST* **6** (2011) P11002, doi:10.1088/1748-0221/6/11/P11002.
- [42] M. Botje et al., “The PDF4LHC Working Group Interim Recommendations”, (2011). arXiv:1101.0538.
- [43] S. Alekhin et al., “The PDF4LHC Working Group Interim Report”, (2011). arXiv:1101.0536.
- [44] NNPDF Collaboration, “Parton distributions for the LHC Run II”, *JHEP* **04** (2015) 040, doi:10.1007/JHEP04(2015)040, arXiv:1410.8849.
- [45] C. G. Lester and D. J. Summers, “Measuring masses of semiinvisibly decaying particles pair produced at hadron colliders”, *Phys. Lett. B* **463** (1999) 99, doi:10.1016/S0370-2693(99)00945-4, arXiv:hep-ph/9906349.

-
- [46] T. Junk, “Confidence level computation for combining searches with small statistics”, *Nucl. Instrum. Meth. A* **434** (1999) 435, doi:10.1016/S0168-9002(99)00498-2, arXiv:hep-ex/9902006.
- [47] A. L. Read, “Presentation of search results: the CL_s technique”, *J. Phys. G* **28** (2002) 2693, doi:10.1088/0954-3899/28/10/313.
- [48] ATLAS and CMS Collaborations, “Procedure for the LHC Higgs boson search combination in summer 2011”, Technical Report ATL-PHYS-PUB-2011-011, CMS-NOTE-2011-005, CERN, 2011.

A The CMS Collaboration

Yerevan Physics Institute, Yerevan, Armenia

V. Khachatryan, A.M. Sirunyan, A. Tumasyan

Institut für Hochenergiephysik der OeAW, Wien, Austria

W. Adam, E. Asilar, T. Bergauer, J. Brandstetter, E. Brondolin, M. Dragicevic, J. Erö, M. Flechl, M. Friedl, R. Frühwirth¹, V.M. Ghete, C. Hartl, N. Hörmann, J. Hrubec, M. Jeitler¹, V. Knünz, A. König, M. Krammer¹, I. Krätschmer, D. Liko, T. Matsushita, I. Mikulec, D. Rabadý², N. Rad, B. Rahbaran, H. Rohringer, J. Schieck¹, R. Schöfbeck, J. Strauss, W. Treberer-Treberspurg, W. Waltenberger, C.-E. Wulz¹

National Centre for Particle and High Energy Physics, Minsk, Belarus

V. Mossolov, N. Shumeiko, J. Suarez Gonzalez

Universiteit Antwerpen, Antwerpen, Belgium

S. Alderweireldt, T. Cornelis, E.A. De Wolf, X. Janssen, A. Knutsson, J. Lauwers, S. Luyckx, M. Van De Klundert, H. Van Haevermaet, P. Van Mechelen, N. Van Remortel, A. Van Spilbeeck

Vrije Universiteit Brussel, Brussel, Belgium

S. Abu Zeid, F. Blekman, J. D'Hondt, N. Daci, I. De Bruyn, K. Deroover, N. Heracleous, J. Keaveney, S. Lowette, L. Moreels, A. Olbrechts, Q. Python, D. Strom, S. Tavernier, W. Van Doninck, P. Van Mulders, G.P. Van Onsem, I. Van Parijs

Université Libre de Bruxelles, Bruxelles, Belgium

P. Barria, H. Brun, C. Caillol, B. Clerbaux, G. De Lentdecker, W. Fang, G. Fasanella, L. Favart, R. Goldouzian, A. Grebenyuk, G. Karapostoli, T. Lenzi, A. Léonard, T. Maerschalk, A. Marinov, L. Perniè, A. Randle-conde, T. Seva, C. Vander Velde, P. Vanlaer, R. Yonamine, F. Zenoni, F. Zhang³

Ghent University, Ghent, Belgium

K. Beernaert, L. Benucci, A. Cimmino, S. Crucy, D. Dobur, A. Fagot, G. Garcia, M. Gul, J. Mccartin, A.A. Ocampo Rios, D. Poyraz, D. Ryckbosch, S. Salva, M. Sigamani, M. Tytgat, W. Van Driessche, E. Yazgan, N. Zaganidis

Université Catholique de Louvain, Louvain-la-Neuve, Belgium

S. Basegmez, C. Beluffi⁴, O. Bondu, S. Brochet, G. Bruno, A. Caudron, L. Ceard, C. Delaere, D. Favart, L. Forthomme, A. Giammanco⁵, A. Jafari, P. Jez, M. Komm, V. Lemaitre, A. Mertens, M. Musich, C. Nuttens, L. Perrini, K. Piotrkowski, A. Popov⁶, L. Quertenmont, M. Selvaggi, M. Vidal Marono

Université de Mons, Mons, Belgium

N. Beliy, G.H. Hammad

Centro Brasileiro de Pesquisas Fisicas, Rio de Janeiro, Brazil

W.L. Aldá Júnior, F.L. Alves, G.A. Alves, L. Brito, M. Correa Martins Junior, M. Hamer, C. Hensel, A. Moraes, M.E. Pol, P. Rebello Teles

Universidade do Estado do Rio de Janeiro, Rio de Janeiro, Brazil

E. Belchior Batista Das Chagas, W. Carvalho, J. Chinellato⁷, A. Custódio, E.M. Da Costa, D. De Jesus Damiao, C. De Oliveira Martins, S. Fonseca De Souza, L.M. Huertas Guativa, H. Malbouisson, D. Matos Figueiredo, C. Mora Herrera, L. Mundim, H. Nogima, W.L. Prado Da Silva, A. Santoro, A. Sznajder, E.J. Tonelli Manganote⁷, A. Vilela Pereira

Universidade Estadual Paulista ^a, Universidade Federal do ABC ^b, São Paulo, Brazil

S. Ahuja^a, C.A. Bernardes^b, A. De Souza Santos^b, S. Dogra^a, T.R. Fernandez Perez Tomei^a, E.M. Gregores^b, P.G. Mercadante^b, C.S. Moon^{a,8}, S.F. Novaes^a, Sandra S. Padula^a, D. Romero Abad, J.C. Ruiz Vargas

Institute for Nuclear Research and Nuclear Energy, Sofia, Bulgaria

A. Aleksandrov, R. Hadjiiska, P. Iaydjiev, M. Rodozov, S. Stoykova, G. Sultanov, M. Vutova

University of Sofia, Sofia, Bulgaria

A. Dimitrov, I. Glushkov, L. Litov, B. Pavlov, P. Petkov

Institute of High Energy Physics, Beijing, China

M. Ahmad, J.G. Bian, G.M. Chen, H.S. Chen, M. Chen, T. Cheng, R. Du, C.H. Jiang, D. Leggat, R. Plestina⁹, F. Romeo, S.M. Shaheen, A. Spiezia, J. Tao, C. Wang, Z. Wang, H. Zhang

State Key Laboratory of Nuclear Physics and Technology, Peking University, Beijing, China

C. Asawatrangkuldee, Y. Ban, Q. Li, S. Liu, Y. Mao, S.J. Qian, D. Wang, Z. Xu

Universidad de Los Andes, Bogota, Colombia

C. Avila, A. Cabrera, L.F. Chaparro Sierra, C. Florez, J.P. Gomez, B. Gomez Moreno, J.C. Sanabria

University of Split, Faculty of Electrical Engineering, Mechanical Engineering and Naval Architecture, Split, Croatia

N. Godinovic, D. Lelas, I. Puljak, P.M. Ribeiro Cipriano

University of Split, Faculty of Science, Split, Croatia

Z. Antunovic, M. Kovac

Institute Rudjer Boskovic, Zagreb, Croatia

V. Brigljevic, K. Kadija, J. Luetic, S. Micanovic, L. Sudic

University of Cyprus, Nicosia, Cyprus

A. Attikis, G. Mavromanolakis, J. Mousa, C. Nicolaou, F. Ptochos, P.A. Razis, H. Rykaczewski

Charles University, Prague, Czech Republic

M. Bodlak, M. Finger¹⁰, M. Finger Jr.¹⁰

Academy of Scientific Research and Technology of the Arab Republic of Egypt, Egyptian Network of High Energy Physics, Cairo, Egypt

Y. Assran^{11,12}, S. Elgammal¹¹, A. Ellithi Kamel^{13,13}, M.A. Mahmoud^{14,11}

National Institute of Chemical Physics and Biophysics, Tallinn, Estonia

B. Calpas, M. Kadastik, M. Murumaa, M. Raidal, A. Tiko, C. Veelken

Department of Physics, University of Helsinki, Helsinki, Finland

P. Eerola, J. Pekkanen, M. Voutilainen

Helsinki Institute of Physics, Helsinki, Finland

J. Härkönen, V. Karimäki, R. Kinnunen, T. Lampén, K. Lassila-Perini, S. Lehti, T. Lindén, P. Luukka, T. Peltola, J. Tuominiemi, E. Tuovinen, L. Wendland

Lappeenranta University of Technology, Lappeenranta, Finland

J. Talvitie, T. Tuuva

DSM/IRFU, CEA/Saclay, Gif-sur-Yvette, France

M. Besancon, F. Couderc, M. Dejardin, D. Denegri, B. Fabbro, J.L. Faure, C. Favaro, F. Ferri,

S. Ganjour, A. Givernaud, P. Gras, G. Hamel de Monchenault, P. Jarry, E. Locci, M. Machet, J. Malcles, J. Rander, A. Rosowsky, M. Titov, A. Zghiche

Laboratoire Leprince-Ringuet, Ecole Polytechnique, IN2P3-CNRS, Palaiseau, France

I. Antropov, S. Baffioni, F. Beaudette, P. Busson, L. Cadamuro, E. Chapon, C. Charlot, O. Davignon, N. Filipovic, R. Granier de Cassagnac, M. Jo, S. Lisniak, L. Mastrolorenzo, P. Miné, I.N. Naranjo, M. Nguyen, C. Ochando, G. Ortona, P. Paganini, P. Pigard, S. Regnard, R. Salerno, J.B. Sauvan, Y. Sirois, T. Strebler, Y. Yilmaz, A. Zabi

Institut Pluridisciplinaire Hubert Curien, Université de Strasbourg, Université de Haute Alsace Mulhouse, CNRS/IN2P3, Strasbourg, France

J.-L. Agram¹⁵, J. Andrea, A. Aubin, D. Bloch, J.-M. Brom, M. Buttignol, E.C. Chabert, N. Chanon, C. Collard, E. Conte¹⁵, X. Coubez, J.-C. Fontaine¹⁵, D. Gelé, U. Goerlach, C. Goetzmann, A.-C. Le Bihan, J.A. Merlin², K. Skovpen, P. Van Hove

Centre de Calcul de l'Institut National de Physique Nucleaire et de Physique des Particules, CNRS/IN2P3, Villeurbanne, France

S. Gadrat

Université de Lyon, Université Claude Bernard Lyon 1, CNRS-IN2P3, Institut de Physique Nucléaire de Lyon, Villeurbanne, France

S. Beauceron, C. Bernet, G. Boudoul, E. Bouvier, C.A. Carrillo Montoya, R. Chierici, D. Contardo, B. Courbon, P. Depasse, H. El Mamouni, J. Fan, J. Fay, S. Gascon, M. Gouzevitch, B. Ille, F. Lagarde, I.B. Laktineh, M. Lethuillier, L. Mirabito, A.L. Pequegnot, S. Perries, J.D. Ruiz Alvarez, D. Sabes, L. Sgandurra, V. Sordini, M. Vander Donckt, P. Verdier, S. Viret

Georgian Technical University, Tbilisi, Georgia

T. Toriashvili¹⁶

Tbilisi State University, Tbilisi, Georgia

Z. Tsamalaidze¹⁰

RWTH Aachen University, I. Physikalisches Institut, Aachen, Germany

C. Autermann, S. Beranek, L. Feld, A. Heister, M.K. Kiesel, K. Klein, M. Lipinski, A. Ostapchuk, M. Preuten, F. Raupach, S. Schael, J.F. Schulte, T. Verlage, H. Weber, V. Zhukov⁶

RWTH Aachen University, III. Physikalisches Institut A, Aachen, Germany

M. Ata, M. Brodski, E. Dietz-Laursonn, D. Duchardt, M. Endres, M. Erdmann, S. Erdweg, T. Esch, R. Fischer, A. Güth, T. Hebbeker, C. Heidemann, K. Hoepfner, S. Knutzen, P. Kreuzer, M. Merschmeyer, A. Meyer, P. Millet, S. Mukherjee, M. Olschewski, K. Padeken, P. Papacz, T. Pook, M. Radziej, H. Reithler, M. Rieger, F. Scheuch, L. Sonnenschein, D. Teyssier, S. Thüer

RWTH Aachen University, III. Physikalisches Institut B, Aachen, Germany

V. Cherepanov, Y. Erdogan, G. Flügge, H. Geenen, M. Geisler, F. Hoehle, B. Kargoll, T. Kress, A. Künsken, J. Lingemann, A. Nehrkorn, A. Nowack, I.M. Nugent, C. Pistone, O. Pooth, A. Stahl

Deutsches Elektronen-Synchrotron, Hamburg, Germany

M. Aldaya Martin, I. Asin, N. Bartosik, O. Behnke, U. Behrens, K. Borras¹⁷, A. Burgmeier, A. Campbell, C. Contreras-Campana, F. Costanza, C. Diez Pardos, G. Dolinska, S. Dooling, T. Dorland, G. Eckerlin, D. Eckstein, T. Eichhorn, G. Flucke, E. Gallo¹⁸, J. Garay Garcia, A. Geiser, A. Gizhko, P. Gunnellini, J. Hauk, M. Hempel¹⁹, H. Jung, A. Kalogeropoulos, O. Karacheban¹⁹, M. Kasemann, P. Katsas, J. Kieseler, C. Kleinwort, I. Korol, D. Krücker, W. Lange, J. Leonard, K. Lipka, A. Lobanov, W. Lohmann¹⁹, R. Mankel, I.-A. Melzer-Pellmann,

A.B. Meyer, G. Mittag, J. Mnich, A. Mussgiller, S. Naumann-Emme, A. Nayak, E. Ntomari, H. Perrey, D. Pitzl, R. Placakyte, A. Raspereza, B. Roland, M.Ö. Sahin, P. Saxena, T. Schoerner-Sadenius, C. Seitz, S. Spannagel, N. Stefaniuk, K.D. Trippkewitz, R. Walsh, C. Wissing

University of Hamburg, Hamburg, Germany

V. Blobel, M. Centis Vignali, A.R. Draeger, J. Erfle, E. Garutti, K. Goebel, D. Gonzalez, M. Görner, J. Haller, M. Hoffmann, R.S. Höing, A. Junkes, R. Klanner, R. Kogler, N. Kovalchuk, T. Lapsien, T. Lenz, I. Marchesini, D. Marconi, M. Meyer, D. Nowatschin, J. Ott, F. Pantaleo², T. Peiffer, A. Perieanu, N. Pietsch, J. Poehlsen, D. Rathjens, C. Sander, C. Scharf, P. Schleper, E. Schlieckau, A. Schmidt, S. Schumann, J. Schwandt, V. Sola, H. Stadie, G. Steinbrück, F.M. Stober, H. Tholen, D. Troendle, E. Usai, L. Vanelderen, A. Vanhoefer, B. Vormwald

Institut für Experimentelle Kernphysik, Karlsruhe, Germany

C. Barth, C. Baus, J. Berger, C. Böser, E. Butz, T. Chwalek, F. Colombo, W. De Boer, A. Descroix, A. Dierlamm, S. Fink, F. Frensch, R. Friese, M. Giffels, A. Gilbert, D. Haitz, F. Hartmann², S.M. Heindl, U. Husemann, I. Katkov⁶, A. Kornmayer², P. Lobelle Pardo, B. Maier, H. Mildner, M.U. Mozer, T. Müller, Th. Müller, M. Plagge, G. Quast, K. Rabbertz, S. Röcker, F. Roscher, M. Schröder, G. Sieber, H.J. Simonis, R. Ulrich, J. Wagner-Kuhr, S. Wayand, M. Weber, T. Weiler, S. Williamson, C. Wöhrmann, R. Wolf

Institute of Nuclear and Particle Physics (INPP), NCSR Demokritos, Aghia Paraskevi, Greece

G. Anagnostou, G. Daskalakis, T. Gerasis, V.A. Giakoumopoulou, A. Kyriakis, D. Loukas, A. Psallidas, I. Topsis-Giotis

National and Kapodistrian University of Athens, Athens, Greece

A. Agapitos, S. Kesisoglou, A. Panagiotou, N. Saoulidou, E. Tziaferi

University of Ioánnina, Ioánnina, Greece

I. Evangelou, G. Flouris, C. Foudas, P. Kokkas, N. Loukas, N. Manthos, I. Papadopoulos, E. Paradas, J. Strologas

Wigner Research Centre for Physics, Budapest, Hungary

G. Bencze, C. Hajdu, A. Hazi, P. Hidas, D. Horvath²⁰, F. Sikler, V. Veszpremi, G. Vesztergombi²¹, A.J. Zsigmond

Institute of Nuclear Research ATOMKI, Debrecen, Hungary

N. Beni, S. Czellar, J. Karancsi²², J. Molnar, Z. Szillasi²

University of Debrecen, Debrecen, Hungary

M. Bartók²³, A. Makovec, P. Raics, Z.L. Trocsanyi, B. Ujvari

National Institute of Science Education and Research, Bhubaneswar, India

S. Choudhury²⁴, P. Mal, K. Mandal, D.K. Sahoo, N. Sahoo, S.K. Swain

Panjab University, Chandigarh, India

S. Bansal, S.B. Beri, V. Bhatnagar, R. Chawla, R. Gupta, U. Bhawandeep, A.K. Kalsi, A. Kaur, M. Kaur, R. Kumar, A. Mehta, M. Mittal, J.B. Singh, G. Walia

University of Delhi, Delhi, India

Ashok Kumar, A. Bhardwaj, B.C. Choudhary, R.B. Garg, S. Malhotra, M. Naimuddin, N. Nishu, K. Ranjan, R. Sharma, V. Sharma

Saha Institute of Nuclear Physics, Kolkata, India

S. Bhattacharya, K. Chatterjee, S. Dey, S. Dutta, N. Majumdar, A. Modak, K. Mondal, S. Mukhopadhyay, A. Roy, D. Roy, S. Roy Chowdhury, S. Sarkar, M. Sharan

Bhabha Atomic Research Centre, Mumbai, India

A. Abdulsalam, R. Chudasama, D. Dutta, V. Jha, V. Kumar, A.K. Mohanty², L.M. Pant, P. Shukla, A. Topkar

Tata Institute of Fundamental Research, Mumbai, India

T. Aziz, S. Banerjee, S. Bhowmik²⁵, R.M. Chatterjee, R.K. Dewanjee, S. Dugad, S. Ganguly, S. Ghosh, M. Guchait, A. Gurtu²⁶, Sa. Jain, G. Kole, S. Kumar, B. Mahakud, M. Maity²⁵, G. Majumder, K. Mazumdar, S. Mitra, G.B. Mohanty, B. Parida, T. Sarkar²⁵, N. Sur, B. Sutar, N. Wickramage²⁷

Indian Institute of Science Education and Research (IISER), Pune, India

S. Chauhan, S. Dube, A. Kapoor, K. Kothekar, S. Sharma

Institute for Research in Fundamental Sciences (IPM), Tehran, Iran

H. Bakhshiansohi, H. Behnamian, S.M. Etesami²⁸, A. Fahim²⁹, M. Khakzad, M. Mohammadi Najafabadi, M. Naseri, S. Paktinat Mehdiabadi, F. Rezaei Hosseinabadi, B. Safarzadeh³⁰, M. Zeinali

University College Dublin, Dublin, Ireland

M. Felcini, M. Grunewald

INFN Sezione di Bari ^a, Università di Bari ^b, Politecnico di Bari ^c, Bari, Italy

M. Abbrescia^{a,b}, C. Calabria^{a,b}, C. Caputo^{a,b}, A. Colaleo^a, D. Creanza^{a,c}, L. Cristella^{a,b}, N. De Filippis^{a,c}, M. De Palma^{a,b}, L. Fiore^a, G. Iaselli^{a,c}, G. Maggi^{a,c}, M. Maggi^a, G. Miniello^{a,b}, S. My^{a,c}, S. Nuzzo^{a,b}, A. Pompili^{a,b}, G. Pugliese^{a,c}, R. Radogna^{a,b}, A. Ranieri^a, G. Selvaggi^{a,b}, L. Silvestris^{a,2}, R. Venditti^{a,b}

INFN Sezione di Bologna ^a, Università di Bologna ^b, Bologna, Italy

G. Abbiendi^a, C. Battilana², D. Bonacorsi^{a,b}, S. Braibant-Giacomelli^{a,b}, L. Brigliadori^{a,b}, R. Campanini^{a,b}, P. Capiluppi^{a,b}, A. Castro^{a,b}, F.R. Cavallo^a, S.S. Chhibra^{a,b}, G. Codispoti^{a,b}, M. Cuffiani^{a,b}, G.M. Dallavalle^a, F. Fabbri^a, A. Fanfani^{a,b}, D. Fasanella^{a,b}, P. Giacomelli^a, C. Grandi^a, L. Guiducci^{a,b}, S. Marcellini^a, G. Masetti^a, A. Montanari^a, F.L. Navarria^{a,b}, A. Perrotta^a, A.M. Rossi^{a,b}, T. Rovelli^{a,b}, G.P. Siroli^{a,b}, N. Tosi^{a,b,2}

INFN Sezione di Catania ^a, Università di Catania ^b, Catania, Italy

G. Cappello^b, M. Chiorboli^{a,b}, S. Costa^{a,b}, A. Di Mattia^a, F. Giordano^{a,b}, R. Potenza^{a,b}, A. Tricomi^{a,b}, C. Tuve^{a,b}

INFN Sezione di Firenze ^a, Università di Firenze ^b, Firenze, Italy

G. Barbagli^a, V. Ciulli^{a,b}, C. Civinini^a, R. D'Alessandro^{a,b}, E. Focardi^{a,b}, V. Gori^{a,b}, P. Lenzi^{a,b}, M. Meschini^a, S. Paoletti^a, G. Sguazzoni^a, L. Viliani^{a,b,2}

INFN Laboratori Nazionali di Frascati, Frascati, Italy

L. Benussi, S. Bianco, F. Fabbri, D. Piccolo, F. Primavera²

INFN Sezione di Genova ^a, Università di Genova ^b, Genova, Italy

V. Calvelli^{a,b}, F. Ferro^a, M. Lo Vetere^{a,b}, M.R. Monge^{a,b}, E. Robutti^a, S. Tosi^{a,b}

INFN Sezione di Milano-Bicocca ^a, Università di Milano-Bicocca ^b, Milano, Italy

L. Brianza, M.E. Dinardo^{a,b}, S. Fiorendi^{a,b}, S. Gennai^a, R. Gerosa^{a,b}, A. Ghezzi^{a,b}, P. Govoni^{a,b},

S. Malvezzi^a, R.A. Manzoni^{a,b,2}, B. Marzocchi^{a,b}, D. Menasce^a, L. Moroni^a, M. Paganoni^{a,b}, D. Pedrini^a, S. Ragazzi^{a,b}, N. Redaelli^a, T. Tabarelli de Fatis^{a,b}

INFN Sezione di Napoli^a, Università di Napoli 'Federico II'^b, Napoli, Italy, Università della Basilicata^c, Potenza, Italy, Università G. Marconi^d, Roma, Italy

S. Buontempo^a, N. Cavallo^{a,c}, S. Di Guida^{a,d,2}, M. Esposito^{a,b}, F. Fabozzi^{a,c}, A.O.M. Iorio^{a,b}, G. Lanza^a, L. Lista^a, S. Meola^{a,d,2}, M. Merola^a, P. Paolucci^{a,2}, C. Sciacca^{a,b}, F. Thyssen

INFN Sezione di Padova^a, Università di Padova^b, Padova, Italy, Università di Trento^c, Trento, Italy

P. Azzi^{a,2}, M. Bellato^a, L. Benato^{a,b}, D. Bisello^{a,b}, A. Boletti^{a,b}, R. Carlin^{a,b}, P. Checchia^a, M. Dall'Osso^{a,b,2}, T. Dorigo^a, U. Dosselli^a, S. Fantinel^a, F. Gasparini^{a,b}, U. Gasparini^{a,b}, F. Gonella^a, A. Gozzelino^a, S. Lacaprara^a, G. Maron^{a,31}, F. Montecassiano^a, M. Passaseo^a, J. Pazzini^{a,b,2}, M. Pegoraro^a, N. Pozzobon^{a,b}, P. Ronchese^{a,b}, M. Tosi^{a,b}, S. Vanini^{a,b}, S. Ventura^a, M. Zanetti, A. Zucchetta^{a,b,2}, G. Zumerle^{a,b}

INFN Sezione di Pavia^a, Università di Pavia^b, Pavia, Italy

A. Braghieri^a, A. Magnani^{a,b}, P. Montagna^{a,b}, S.P. Ratti^{a,b}, V. Re^a, C. Riccardi^{a,b}, P. Salvini^a, I. Vai^{a,b}, P. Vitulo^{a,b}

INFN Sezione di Perugia^a, Università di Perugia^b, Perugia, Italy

L. Alunni Solestizi^{a,b}, G.M. Bilei^a, D. Ciangottini^{a,b,2}, L. Fanò^{a,b}, P. Lariccia^{a,b}, G. Mantovani^{a,b}, M. Menichelli^a, A. Saha^a, A. Santocchia^{a,b}

INFN Sezione di Pisa^a, Università di Pisa^b, Scuola Normale Superiore di Pisa^c, Pisa, Italy

K. Androsov^{a,32}, P. Azzurri^{a,2}, G. Bagliesi^a, J. Bernardini^a, T. Boccali^a, R. Castaldi^a, M.A. Ciocci^{a,32}, R. Dell'Orso^a, S. Donato^{a,c,2}, G. Fedi, L. Foà^{a,c†}, A. Giassi^a, M.T. Grippo^{a,32}, F. Ligabue^{a,c}, T. Lomtadze^a, L. Martini^{a,b}, A. Messineo^{a,b}, F. Palla^a, A. Rizzi^{a,b}, A. Savoy-Navarro^{a,33}, A.T. Serban^a, P. Spagnolo^a, R. Tenchini^a, G. Tonelli^{a,b}, A. Venturi^a, P.G. Verdini^a

INFN Sezione di Roma^a, Università di Roma^b, Roma, Italy

L. Barone^{a,b}, F. Cavallari^a, G. D'imperio^{a,b,2}, D. Del Re^{a,b,2}, M. Diemoz^a, S. Gelli^{a,b}, C. Jorda^a, E. Longo^{a,b}, F. Margaroli^{a,b}, P. Meridiani^a, G. Organtini^{a,b}, R. Paramatti^a, F. Preiato^{a,b}, S. Rahatlou^{a,b}, C. Rovelli^a, F. Santanastasio^{a,b}, P. Traczyk^{a,b,2}

INFN Sezione di Torino^a, Università di Torino^b, Torino, Italy, Università del Piemonte Orientale^c, Novara, Italy

N. Amapane^{a,b}, R. Arcidiacono^{a,c,2}, S. Argiro^{a,b}, M. Arneodo^{a,c}, R. Bellan^{a,b}, C. Biino^a, N. Cartiglia^a, M. Costa^{a,b}, R. Covarelli^{a,b}, A. Degano^{a,b}, N. Demaria^a, L. Finco^{a,b,2}, B. Kiani^{a,b}, C. Mariotti^a, S. Maselli^a, E. Migliore^{a,b}, V. Monaco^{a,b}, E. Monteil^{a,b}, M.M. Obertino^{a,b}, L. Pacher^{a,b}, N. Pastrone^a, M. Pelliccioni^a, G.L. Pinna Angioni^{a,b}, F. Ravera^{a,b}, A. Romero^{a,b}, M. Ruspa^{a,c}, R. Sacchi^{a,b}, A. Solano^{a,b}, A. Staiano^a

INFN Sezione di Trieste^a, Università di Trieste^b, Trieste, Italy

S. Belforte^a, V. Candelise^{a,b}, M. Casarsa^a, F. Cossutti^a, G. Della Ricca^{a,b}, B. Gobbo^a, C. La Licata^{a,b}, M. Marone^{a,b}, A. Schizzi^{a,b}, A. Zanetti^a

Kangwon National University, Chunchon, Korea

A. Kropivnitskaya, S.K. Nam

Kyungpook National University, Daegu, Korea

D.H. Kim, G.N. Kim, M.S. Kim, D.J. Kong, S. Lee, Y.D. Oh, A. Sakharov, D.C. Son

Chonbuk National University, Jeonju, Korea

J.A. Brochero Cifuentes, H. Kim, T.J. Kim

Chonnam National University, Institute for Universe and Elementary Particles, Kwangju, Korea

S. Song

Korea University, Seoul, Korea

S. Cho, S. Choi, Y. Go, D. Gyun, B. Hong, H. Kim, Y. Kim, B. Lee, K. Lee, K.S. Lee, S. Lee, J. Lim, S.K. Park, Y. Roh

Seoul National University, Seoul, Korea

H.D. Yoo

University of Seoul, Seoul, Korea

M. Choi, H. Kim, J.H. Kim, J.S.H. Lee, I.C. Park, G. Ryu, M.S. Ryu

Sungkyunkwan University, Suwon, Korea

Y. Choi, J. Goh, D. Kim, E. Kwon, J. Lee, I. Yu

Vilnius University, Vilnius, Lithuania

V. Dudenas, A. Juodagalvis, J. Vaitkus

National Centre for Particle Physics, Universiti Malaya, Kuala Lumpur, Malaysia

I. Ahmed, Z.A. Ibrahim, J.R. Komaragiri, M.A.B. Md Ali³⁴, F. Mohamad Idris³⁵, W.A.T. Wan Abdullah, M.N. Yusli, Z. Zolkapli

Centro de Investigacion y de Estudios Avanzados del IPN, Mexico City, Mexico

E. Casimiro Linares, H. Castilla-Valdez, E. De La Cruz-Burelo, I. Heredia-De La Cruz³⁶, A. Hernandez-Almada, R. Lopez-Fernandez, A. Sanchez-Hernandez

Universidad Iberoamericana, Mexico City, Mexico

S. Carrillo Moreno, F. Vazquez Valencia

Benemerita Universidad Autonoma de Puebla, Puebla, Mexico

I. Pedraza, H.A. Salazar Ibarguen, C. Uribe Estrada

Universidad Autónoma de San Luis Potosí, San Luis Potosí, Mexico

A. Morelos Pineda

University of Auckland, Auckland, New Zealand

D. Krofcheck

University of Canterbury, Christchurch, New Zealand

P.H. Butler

National Centre for Physics, Quaid-I-Azam University, Islamabad, Pakistan

A. Ahmad, M. Ahmad, Q. Hassan, H.R. Hoorani, W.A. Khan, T. Khurshid, M. Shoaib, M. Waqas

National Centre for Nuclear Research, Swierk, Poland

H. Bialkowska, M. Bluj, B. Boimska, T. Frueboes, M. Górski, M. Kazana, K. Nawrocki, K. Romanowska-Rybinska, M. Szleper, P. Zalewski

Institute of Experimental Physics, Faculty of Physics, University of Warsaw, Warsaw, Poland

G. Brona, K. Bunkowski, A. Byszek³⁷, K. Doroba, A. Kalinowski, M. Konecki, J. Krolikowski, M. Misiura, M. Olszewski, M. Walczak

Laboratório de Instrumentação e Física Experimental de Partículas, Lisboa, Portugal

P. Bargassa, C. Beirão Da Cruz E Silva, A. Di Francesco, P. Faccioli, P.G. Ferreira Parracho,

M. Gallinaro, J. Hollar, N. Leonardo, L. Lloret Iglesias, F. Nguyen, J. Rodrigues Antunes, J. Seixas, O. Toldaiev, D. Vadrucio, J. Varela, P. Vischia

Joint Institute for Nuclear Research, Dubna, Russia

S. Afanasiev, P. Bunin, M. Gavrilenko, I. Golutvin, I. Gorbunov, A. Kamenev, V. Karjavin, A. Lanev, A. Malakhov, V. Matveev^{38,39}, P. Moisezenz, V. Palichik, V. Perelygin, S. Shmatov, S. Shulha, N. Skatchkov, V. Smirnov, A. Zarubin

Petersburg Nuclear Physics Institute, Gatchina (St. Petersburg), Russia

V. Golovtsov, Y. Ivanov, V. Kim⁴⁰, E. Kuznetsova, P. Levchenko, V. Murzin, V. Oreshkin, I. Smirnov, V. Sulimov, L. Uvarov, S. Vavilov, A. Vorobyev

Institute for Nuclear Research, Moscow, Russia

Yu. Andreev, A. Dermenev, S. Gninenko, N. Golubev, A. Karneyeu, M. Kirsanov, N. Krasnikov, A. Pashenkov, D. Tlisov, A. Toropin

Institute for Theoretical and Experimental Physics, Moscow, Russia

V. Epshteyn, V. Gavrillov, N. Lychkovskaya, V. Popov, I. Pozdnyakov, G. Safronov, A. Spiridonov, E. Vlasov, A. Zhokin

National Research Nuclear University 'Moscow Engineering Physics Institute' (MEPhI), Moscow, Russia

M. Chadeeva, R. Chistov, M. Danilov, V. Rusinov, E. Tarkovskii

P.N. Lebedev Physical Institute, Moscow, Russia

V. Andreev, M. Azarkin³⁹, I. Dremin³⁹, M. Kirakosyan, A. Leonidov³⁹, G. Mesyats, S.V. Rusakov

Skobeltsyn Institute of Nuclear Physics, Lomonosov Moscow State University, Moscow, Russia

A. Baskakov, A. Belyaev, E. Boos, M. Dubinin⁴¹, L. Dudko, A. Ershov, A. Gribushin, V. Klyukhin, O. Kodolova, I. Lokhtin, I. Miagkov, S. Obraztsov, S. Petrushanko, V. Savrin, A. Snigirev

State Research Center of Russian Federation, Institute for High Energy Physics, Protvino, Russia

I. Azhgirey, I. Bayshev, S. Bitioukov, V. Kachanov, A. Kalinin, D. Konstantinov, V. Krychkin, V. Petrov, R. Ryutin, A. Sobol, L. Tourtchanovitch, S. Troshin, N. Tyurin, A. Uzunian, A. Volkov

University of Belgrade, Faculty of Physics and Vinca Institute of Nuclear Sciences, Belgrade, Serbia

P. Adzic⁴², P. Cirkovic, D. Devetak, J. Milosevic, V. Rekovic

Centro de Investigaciones Energéticas Medioambientales y Tecnológicas (CIEMAT), Madrid, Spain

J. Alcaraz Maestre, E. Calvo, M. Cerrada, M. Chamizo Llatas, N. Colino, B. De La Cruz, A. Delgado Peris, A. Escalante Del Valle, C. Fernandez Bedoya, J.P. Fernández Ramos, J. Flix, M.C. Fouz, P. Garcia-Abia, O. Gonzalez Lopez, S. Goy Lopez, J.M. Hernandez, M.I. Josa, E. Navarro De Martino, A. Pérez-Calero Yzquierdo, J. Puerta Pelayo, A. Quintario Olmeda, I. Redondo, L. Romero, J. Santaolalla, M.S. Soares

Universidad Autónoma de Madrid, Madrid, Spain

C. Albajar, J.F. de Trocóniz, M. Missiroli, D. Moran

Universidad de Oviedo, Oviedo, Spain

J. Cuevas, J. Fernandez Menendez, S. Folgueras, I. Gonzalez Caballero, E. Palencia Cortezon, J.M. Vizan Garcia

Instituto de Física de Cantabria (IFCA), CSIC-Universidad de Cantabria, Santander, Spain

I.J. Cabrillo, A. Calderon, J.R. Castiñeiras De Saa, P. De Castro Manzano, M. Fernandez, J. Garcia-Ferrero, G. Gomez, A. Lopez Virto, J. Marco, R. Marco, C. Martinez Rivero, F. Matorras, J. Piedra Gomez, T. Rodrigo, A.Y. Rodríguez-Marrero, A. Ruiz-Jimeno, L. Scodellaro, N. Trevisani, I. Vila, R. Vilar Cortabitarte

CERN, European Organization for Nuclear Research, Geneva, Switzerland

D. Abbaneo, E. Auffray, G. Auzinger, M. Bachtis, P. Baillon, A.H. Ball, D. Barney, A. Benaglia, J. Bendavid, L. Benhabib, G.M. Berruti, P. Bloch, A. Bocci, A. Bonato, C. Botta, H. Breuker, T. Camporesi, R. Castello, G. Cerminara, M. D'Alfonso, D. d'Enterria, A. Dabrowski, V. Daponte, A. David, M. De Gruttola, F. De Guio, A. De Roeck, S. De Visscher, E. Di Marco⁴³, M. Dobson, M. Dordevic, B. Dorney, T. du Pree, D. Duggan, M. Dünser, N. Dupont, A. Elliott-Peisert, G. Franzoni, J. Fulcher, W. Funk, D. Gigi, K. Gill, D. Giordano, M. Girone, F. Glege, R. Guida, S. Gundacker, M. Guthoff, J. Hammer, P. Harris, J. Hegeman, V. Innocente, P. Janot, H. Kirschenmann, M.J. Kortelainen, K. Kousouris, K. Krajczar, P. Lecoq, C. Lourenço, M.T. Lucchini, N. Magini, L. Malgeri, M. Mannelli, A. Martelli, L. Masetti, F. Meijers, S. Mersi, E. Meschi, F. Moortgat, S. Morovic, M. Mulders, M.V. Nemallapudi, H. Neugebauer, S. Orfanelli⁴⁴, L. Orsini, L. Pape, E. Perez, M. Peruzzi, A. Petrilli, G. Petrucciani, A. Pfeiffer, M. Pierini, D. Piparo, A. Racz, T. Reis, G. Rolandi⁴⁵, M. Rovere, M. Ruan, H. Sakulin, C. Schäfer, C. Schwick, M. Seidel, A. Sharma, P. Silva, M. Simon, P. Sphicas⁴⁶, J. Steggemann, B. Stieger, M. Stoye, Y. Takahashi, D. Treille, A. Triossi, A. Tsiros, G.I. Veres²¹, N. Wardle, H.K. Wöhri, A. Zagozdinska³⁷, W.D. Zeuner

Paul Scherrer Institut, Villigen, Switzerland

W. Bertl, K. Deiters, W. Erdmann, R. Horisberger, Q. Ingram, H.C. Kaestli, D. Kotlinski, U. Langenegger, T. Rohe

Institute for Particle Physics, ETH Zurich, Zurich, Switzerland

F. Bachmair, L. Bäni, L. Bianchini, B. Casal, G. Dissertori, M. Dittmar, M. Donegà, P. Eller, C. Grab, C. Heidegger, D. Hits, J. Hoss, G. Kasieczka, P. Lecomte[†], W. Lustermann, B. Mangano, M. Marionneau, P. Martinez Ruiz del Arbol, M. Masciovecchio, M.T. Meinhard, D. Meister, F. Micheli, P. Musella, F. Nessi-Tedaldi, F. Pandolfi, J. Pata, F. Pauss, L. Perrozzi, M. Quittnat, M. Rossini, M. Schönenberger, A. Starodumov⁴⁷, M. Takahashi, V.R. Tavolaro, K. Theofilatos, R. Wallny

Universität Zürich, Zurich, Switzerland

T.K. Aarrestad, C. Amsler⁴⁸, L. Caminada, M.F. Canelli, V. Chiochia, A. De Cosa, C. Galloni, A. Hinzmann, T. Hreus, B. Kilminster, C. Lange, J. Ngadiuba, D. Pinna, G. Rauco, P. Robmann, D. Salerno, Y. Yang

National Central University, Chung-Li, Taiwan

M. Cardaci, K.H. Chen, T.H. Doan, Sh. Jain, R. Khurana, M. Konyushikhin, C.M. Kuo, W. Lin, Y.J. Lu, A. Pozdnyakov, S.S. Yu

National Taiwan University (NTU), Taipei, Taiwan

Arun Kumar, P. Chang, Y.H. Chang, Y.W. Chang, Y. Chao, K.F. Chen, P.H. Chen, C. Dietz, F. Fiori, U. Grundler, W.-S. Hou, Y. Hsiung, Y.F. Liu, R.-S. Lu, M. Miñano Moya, E. Petrakou, J.f. Tsai, Y.M. Tzeng

Chulalongkorn University, Faculty of Science, Department of Physics, Bangkok, Thailand

B. Asavapibhop, K. Kovitanggoon, G. Singh, N. Srimanobhas, N. Suwonjandee

Cukurova University, Adana, Turkey

A. Adiguzel, S. Cerci⁴⁹, S. Damarseckin, Z.S. Demiroglu, C. Dozen, I. Dumanoglu, F.H. Gecit, S. Girgis, G. Gokbulut, Y. Guler, E. Gurpinar, I. Hos, E.E. Kangal⁵⁰, A. Kayis Topaksu, G. Onengut⁵¹, M. Ozcan, K. Ozdemir⁵², S. Ozturk⁵³, A. Polatoz, B. Tali⁴⁹, C. Zorbilmez

Middle East Technical University, Physics Department, Ankara, Turkey

B. Bilin, S. Bilmis, B. Isildak⁵⁴, G. Karapinar⁵⁵, M. Yalvac, M. Zeyrek

Bogazici University, Istanbul, Turkey

E. Gülmez, M. Kaya⁵⁶, O. Kaya⁵⁷, E.A. Yetkin⁵⁸, T. Yetkin⁵⁹

Istanbul Technical University, Istanbul, Turkey

A. Cakir, K. Cankocak, S. Sen⁶⁰, F.I. Vardarli

Institute for Scintillation Materials of National Academy of Science of Ukraine, Kharkov, Ukraine

B. Grynyov

National Scientific Center, Kharkov Institute of Physics and Technology, Kharkov, Ukraine

L. Levchuk, P. Sorokin

University of Bristol, Bristol, United Kingdom

R. Aggleton, F. Ball, L. Beck, J.J. Brooke, E. Clement, D. Cussans, H. Flacher, J. Goldstein, M. Grimes, G.P. Heath, H.F. Heath, J. Jacob, L. Kreczko, C. Lucas, Z. Meng, D.M. Newbold⁶¹, S. Paramesvaran, A. Poll, T. Sakuma, S. Seif El Nasr-storey, S. Senkin, D. Smith, V.J. Smith

Rutherford Appleton Laboratory, Didcot, United Kingdom

K.W. Bell, A. Belyaev⁶², C. Brew, R.M. Brown, L. Calligaris, D. Cieri, D.J.A. Cockerill, J.A. Coughlan, K. Harder, S. Harper, E. Olaiya, D. Petyt, C.H. Shepherd-Themistocleous, A. Thea, I.R. Tomalin, T. Williams, S.D. Worm

Imperial College, London, United Kingdom

M. Baber, R. Bainbridge, O. Buchmuller, A. Bundock, D. Burton, S. Casasso, M. Citron, D. Colling, L. Corpe, P. Dauncey, G. Davies, A. De Wit, M. Della Negra, P. Dunne, A. Elwood, D. Futyan, G. Hall, G. Iles, R. Lane, R. Lucas⁶¹, L. Lyons, A.-M. Magnan, S. Malik, J. Nash, A. Nikitenko⁴⁷, J. Pela, M. Pesaresi, D.M. Raymond, A. Richards, A. Rose, C. Seez, A. Tapper, K. Uchida, M. Vazquez Acosta⁶³, T. Virdee, S.C. Zenz

Brunel University, Uxbridge, United Kingdom

J.E. Cole, P.R. Hobson, A. Khan, P. Kyberd, D. Leslie, I.D. Reid, P. Symonds, L. Teodorescu, M. Turner

Baylor University, Waco, USA

A. Borzou, K. Call, J. Dittmann, K. Hatakeyama, H. Liu, N. Pastika

The University of Alabama, Tuscaloosa, USA

O. Charaf, S.I. Cooper, C. Henderson, P. Rumerio

Boston University, Boston, USA

D. Arcaro, A. Avetisyan, T. Bose, D. Gastler, D. Rankin, C. Richardson, J. Rohlf, L. Sulak, D. Zou

Brown University, Providence, USA

J. Alimena, G. Benelli, E. Berry, D. Cutts, A. Ferapontov, A. Garabedian, J. Hakala, U. Heintz, O. Jesus, E. Laird, G. Landsberg, Z. Mao, M. Narain, S. Piperov, S. Sagir, R. Syarif

University of California, Davis, Davis, USA

R. Breedon, G. Breto, M. Calderon De La Barca Sanchez, S. Chauhan, M. Chertok, J. Conway, R. Conway, P.T. Cox, R. Erbacher, G. Funk, M. Gardner, W. Ko, R. Lander, C. Mclean, M. Mulhearn, D. Pellett, J. Pilot, F. Ricci-Tam, S. Shalhout, J. Smith, M. Squires, D. Stolp, M. Tripathi, S. Wilbur, R. Yohay

University of California, Los Angeles, USA

R. Cousins, P. Everaerts, A. Florent, J. Hauser, M. Ignatenko, D. Saltzberg, E. Takasugi, V. Valuev, M. Weber

University of California, Riverside, Riverside, USA

K. Burt, R. Clare, J. Ellison, J.W. Gary, G. Hanson, J. Heilman, M. Ivova PANEVA, P. Jandir, E. Kennedy, F. Lacroix, O.R. Long, M. Malberti, M. Olmedo Negrete, A. Shrinivas, H. Wei, S. Wimpenny, B. R. Yates

University of California, San Diego, La Jolla, USA

J.G. Branson, G.B. Cerati, S. Cittolin, R.T. D'Agnolo, M. Derdzinski, A. Holzner, R. Kelley, D. Klein, J. Letts, I. Macneill, D. Olivito, S. Padhi, M. Pieri, M. Sani, V. Sharma, S. Simon, M. Tadel, A. Vartak, S. Wasserbaech⁶⁴, C. Welke, F. Würthwein, A. Yagil, G. Zevi Della Porta

University of California, Santa Barbara, Santa Barbara, USA

J. Bradmiller-Feld, C. Campagnari, A. Dishaw, V. Dutta, K. Flowers, M. Franco Sevilla, P. Geffert, C. George, F. Golf, L. Gouskos, J. Gran, J. Incandela, N. Mccoll, S.D. Mullin, J. Richman, D. Stuart, I. Suarez, C. West, J. Yoo

California Institute of Technology, Pasadena, USA

D. Anderson, A. Apresyan, A. Bornheim, J. Bunn, Y. Chen, J. Duarte, A. Mott, H.B. Newman, C. Pena, M. Spiropulu, J.R. Vlimant, S. Xie, R.Y. Zhu

Carnegie Mellon University, Pittsburgh, USA

M.B. Andrews, V. Azzolini, A. Calamba, B. Carlson, T. Ferguson, M. Paulini, J. Russ, M. Sun, H. Vogel, I. Vorobiev

University of Colorado Boulder, Boulder, USA

J.P. Cumalat, W.T. Ford, A. Gaz, F. Jensen, A. Johnson, M. Krohn, T. Mulholland, U. Nauenberg, K. Stenson, S.R. Wagner

Cornell University, Ithaca, USA

J. Alexander, A. Chatterjee, J. Chaves, J. Chu, S. Dittmer, N. Eggert, N. Mirman, G. Nicolas Kaufman, J.R. Patterson, A. Rinkevicius, A. Ryd, L. Skinnari, L. Soffi, W. Sun, S.M. Tan, W.D. Teo, J. Thom, J. Thompson, J. Tucker, Y. Weng, P. Wittich

Fermi National Accelerator Laboratory, Batavia, USA

S. Abdullin, M. Albrow, G. Apollinari, S. Banerjee, L.A.T. Bauerdick, A. Beretvas, J. Berryhill, P.C. Bhat, G. Bolla, K. Burkett, J.N. Butler, H.W.K. Cheung, F. Chlebana, S. Cihangir, V.D. Elvira, I. Fisk, J. Freeman, Z. Gecse, E. Gottschalk, L. Gray, D. Green, S. Grünendahl, O. Gutsche, J. Hanlon, D. Hare, R.M. Harris, S. Hasegawa, J. Hirschauer, Z. Hu, B. Jayatilaka, S. Jindariani, M. Johnson, U. Joshi, B. Klima, B. Kreis, S. Lammel, J. Lewis, J. Linacre, D. Lincoln, R. Lipton, T. Liu, R. Lopes De Sá, J. Lykken, K. Maeshima, J.M. Marraffino, S. Maruyama, D. Mason, P. McBride, P. Merkel, S. Mrenna, S. Nahn, C. Newman-Holmes[†], V. O'Dell, K. Pedro,

O. Prokofyev, G. Rakness, E. Sexton-Kennedy, A. Soha, W.J. Spalding, L. Spiegel, S. Stoynev, N. Strobbe, L. Taylor, S. Tkaczyk, N.V. Tran, L. Uplegger, E.W. Vaandering, C. Vernieri, M. Verzocchi, R. Vidal, M. Wang, H.A. Weber, A. Whitbeck

University of Florida, Gainesville, USA

D. Acosta, P. Avery, P. Bortignon, D. Bourilkov, A. Brinkerhoff, A. Carnes, M. Carver, D. Curry, S. Das, R.D. Field, I.K. Furic, J. Konigsberg, A. Korytov, K. Kotov, P. Ma, K. Matchev, H. Mei, P. Milenovic⁶⁵, G. Mitselmakher, D. Rank, R. Rossin, L. Shchutska, M. Snowball, D. Sperka, N. Terentyev, L. Thomas, J. Wang, S. Wang, J. Yelton

Florida International University, Miami, USA

S. Hewamanage, S. Linn, P. Markowitz, G. Martinez, J.L. Rodriguez

Florida State University, Tallahassee, USA

A. Ackert, J.R. Adams, T. Adams, A. Askew, S. Bein, J. Bochenek, B. Diamond, J. Haas, S. Hagopian, V. Hagopian, K.F. Johnson, A. Khatiwada, H. Prosper, M. Weinberg

Florida Institute of Technology, Melbourne, USA

M.M. Baarmand, V. Bhopatkar, S. Colafranceschi⁶⁶, M. Hohlmann, H. Kalakhety, D. Noonan, T. Roy, F. Yumiceva

University of Illinois at Chicago (UIC), Chicago, USA

M.R. Adams, L. Apanasevich, D. Berry, R.R. Betts, I. Bucinskaite, R. Cavanaugh, O. Evdokimov, L. Gauthier, C.E. Gerber, D.J. Hofman, P. Kurt, C. O'Brien, I.D. Sandoval Gonzalez, P. Turner, N. Varelas, Z. Wu, M. Zakaria, J. Zhang

The University of Iowa, Iowa City, USA

B. Bilki⁶⁷, W. Clarida, K. Dilsiz, S. Durgut, R.P. Gandrajula, M. Haytmyradov, V. Khristenko, J.-P. Merlo, H. Mermerkaya⁶⁸, A. Mestvirishvili, A. Moeller, J. Nachtman, H. Ogul, Y. Onel, F. Ozok⁶⁹, A. Penzo, C. Snyder, E. Tiras, J. Wetzel, K. Yi

Johns Hopkins University, Baltimore, USA

I. Anderson, B.A. Barnett, B. Blumenfeld, N. Eminizer, D. Fehling, L. Feng, A.V. Gritsan, P. Maksimovic, M. Osherson, J. Roskes, A. Sady, U. Sarica, M. Swartz, M. Xiao, Y. Xin, C. You

The University of Kansas, Lawrence, USA

P. Baringer, A. Bean, C. Bruner, R.P. Kenny III, D. Majumder, M. Malek, W. Mcbrayer, M. Murray, S. Sanders, R. Stringer, Q. Wang

Kansas State University, Manhattan, USA

A. Ivanov, K. Kaadze, S. Khalil, M. Makouski, Y. Maravin, A. Mohammadi, L.K. Saini, N. Skhirtladze, S. Toda

Lawrence Livermore National Laboratory, Livermore, USA

D. Lange, F. Rebassoo, D. Wright

University of Maryland, College Park, USA

C. Anelli, A. Baden, O. Baron, A. Belloni, B. Calvert, S.C. Eno, C. Ferraioli, J.A. Gomez, N.J. Hadley, S. Jabeen, R.G. Kellogg, T. Kolberg, J. Kunkle, Y. Lu, A.C. Mignerey, Y.H. Shin, A. Skuja, M.B. Tonjes, S.C. Tonwar

Massachusetts Institute of Technology, Cambridge, USA

A. Apyan, R. Barbieri, A. Baty, R. Bi, K. Bierwagen, S. Brandt, W. Busza, I.A. Cali, Z. Demiragli, L. Di Matteo, G. Gomez Ceballos, M. Goncharov, D. Gulhan, Y. Iiyama, G.M. Innocenti, M. Klute, D. Kovalskyi, Y.S. Lai, Y.-J. Lee, A. Levin, P.D. Luckey, A.C. Marini, C. Mcginn,

C. Mironov, S. Narayanan, X. Niu, C. Paus, C. Roland, G. Roland, J. Salfeld-Nebgen, G.S.F. Stephans, K. Sumorok, M. Varma, D. Velicanu, J. Veverka, J. Wang, T.W. Wang, B. Wyslouch, M. Yang, V. Zhukova

University of Minnesota, Minneapolis, USA

A.C. Benvenuti, B. Dahmes, A. Evans, A. Finkel, A. Gude, P. Hansen, S. Kalafut, S.C. Kao, K. Klapoetke, Y. Kubota, Z. Lesko, J. Mans, S. Nourbakhsh, N. Ruckstuhl, R. Rusack, N. Tambe, J. Turkewitz

University of Mississippi, Oxford, USA

J.G. Acosta, S. Oliveros

University of Nebraska-Lincoln, Lincoln, USA

E. Avdeeva, R. Bartek, K. Bloom, S. Bose, D.R. Claes, A. Dominguez, C. Fangmeier, R. Gonzalez Suarez, R. Kamalieddin, D. Knowlton, I. Kravchenko, F. Meier, J. Monroy, F. Ratnikov, J.E. Siado, G.R. Snow

State University of New York at Buffalo, Buffalo, USA

M. Alyari, J. Dolen, J. George, A. Godshalk, C. Harrington, I. Iashvili, J. Kaisen, A. Kharchilava, A. Kumar, S. Rappoccio, B. Roozbahani

Northeastern University, Boston, USA

G. Alverson, E. Barberis, D. Baumgartel, M. Chasco, A. Hortiangtham, A. Massironi, D.M. Morse, D. Nash, T. Orimoto, R. Teixeira De Lima, D. Trocino, R.-J. Wang, D. Wood, J. Zhang

Northwestern University, Evanston, USA

S. Bhattacharya, K.A. Hahn, A. Kubik, J.F. Low, N. Mucia, N. Odell, B. Pollack, M. Schmitt, K. Sung, M. Trovato, M. Velasco

University of Notre Dame, Notre Dame, USA

N. Dev, M. Hildreth, C. Jessop, D.J. Karmgard, N. Kellams, K. Lannon, N. Marinelli, F. Meng, C. Mueller, Y. Musienko³⁸, M. Planer, A. Reinsvold, R. Ruchti, G. Smith, S. Taroni, N. Valls, M. Wayne, M. Wolf, A. Woodard

The Ohio State University, Columbus, USA

L. Antonelli, J. Brinson, B. Bylsma, L.S. Durkin, S. Flowers, A. Hart, C. Hill, R. Hughes, W. Ji, T.Y. Ling, B. Liu, W. Luo, D. Puigh, M. Rodenburg, B.L. Winer, H.W. Wulsin

Princeton University, Princeton, USA

O. Driga, P. Elmer, J. Hardenbrook, P. Hebda, S.A. Koay, P. Lujan, D. Marlow, T. Medvedeva, M. Mooney, J. Olsen, C. Palmer, P. Piroué, D. Stickland, C. Tully, A. Zuranski

University of Puerto Rico, Mayaguez, USA

S. Malik

Purdue University, West Lafayette, USA

A. Barker, V.E. Barnes, D. Benedetti, D. Bortoletto, L. Gutay, M.K. Jha, M. Jones, A.W. Jung, K. Jung, A. Kumar, D.H. Miller, N. Neumeister, B.C. Radburn-Smith, X. Shi, I. Shipsey, D. Silvers, J. Sun, A. Svyatkovskiy, F. Wang, W. Xie, L. Xu

Purdue University Calumet, Hammond, USA

N. Parashar, J. Stupak

Rice University, Houston, USA

A. Adair, B. Akgun, Z. Chen, K.M. Ecklund, F.J.M. Geurts, M. Guilbaud, W. Li, B. Michlin, M. Northup, B.P. Padley, R. Redjimi, J. Roberts, J. Rorie, Z. Tu, J. Zabel

University of Rochester, Rochester, USA

B. Betchart, A. Bodek, P. de Barbaro, R. Demina, Y. Eshaq, T. Ferbel, M. Galanti, A. Garcia-Bellido, J. Han, O. Hindrichs, A. Khukhunaishvili, K.H. Lo, P. Tan, M. Verzetti

Rutgers, The State University of New Jersey, Piscataway, USA

J.P. Chou, E. Contreras-Campana, D. Ferencek, Y. Gershtein, E. Halkiadakis, M. Heindl, D. Hidas, E. Hughes, S. Kaplan, R. Kunnawalkam Elayavalli, A. Lath, K. Nash, H. Saka, S. Salur, S. Schnetzer, D. Sheffield, S. Somalwar, R. Stone, S. Thomas, P. Thomassen, M. Walker

University of Tennessee, Knoxville, USA

M. Foerster, G. Riley, K. Rose, S. Spanier, K. Thapa

Texas A&M University, College Station, USA

O. Bouhali⁷⁰, A. Castaneda Hernandez⁷⁰, A. Celik, M. Dalchenko, M. De Mattia, A. Delgado, S. Dildick, R. Eusebi, J. Gilmore, T. Huang, T. Kamon⁷¹, V. Krutelyov, R. Mueller, I. Osipenkov, Y. Pakhotin, R. Patel, A. Perloff, A. Rose, A. Safonov, A. Tatarinov, K.A. Ulmer²

Texas Tech University, Lubbock, USA

N. Akchurin, C. Cowden, J. Damgov, C. Dragoiu, P.R. Duderu, J. Faulkner, S. Kunori, K. Lamichhane, S.W. Lee, T. Libeiro, S. Undleeb, I. Volobouev

Vanderbilt University, Nashville, USA

E. Appelt, A.G. Delannoy, S. Greene, A. Gurrola, R. Janjam, W. Johns, C. Maguire, Y. Mao, A. Melo, H. Ni, P. Sheldon, S. Tuo, J. Velkovska, Q. Xu

University of Virginia, Charlottesville, USA

M.W. Arenton, B. Cox, B. Francis, J. Goodell, R. Hirosky, A. Ledovskoy, H. Li, C. Lin, C. Neu, T. Sinthuprasith, X. Sun, Y. Wang, E. Wolfe, J. Wood, F. Xia

Wayne State University, Detroit, USA

C. Clarke, R. Harr, P.E. Karchin, C. Kottachchi Kankanamge Don, P. Lamichhane, J. Sturdy

University of Wisconsin - Madison, Madison, WI, USA

D.A. Belknap, D. Carlsmith, M. Cepeda, S. Dasu, L. Dodd, S. Duric, B. Gomber, M. Grothe, M. Herndon, A. Hervé, P. Klabbers, A. Lanaro, A. Levine, K. Long, R. Loveless, A. Mohapatra, I. Ojalvo, T. Perry, G.A. Pierro, G. Polese, T. Ruggles, T. Sarangi, A. Savin, A. Sharma, N. Smith, W.H. Smith, D. Taylor, P. Verwilligen, N. Woods

†: Deceased

1: Also at Vienna University of Technology, Vienna, Austria

2: Also at CERN, European Organization for Nuclear Research, Geneva, Switzerland

3: Also at State Key Laboratory of Nuclear Physics and Technology, Peking University, Beijing, China

4: Also at Institut Pluridisciplinaire Hubert Curien, Université de Strasbourg, Université de Haute Alsace Mulhouse, CNRS/IN2P3, Strasbourg, France

5: Also at National Institute of Chemical Physics and Biophysics, Tallinn, Estonia

6: Also at Skobeltsyn Institute of Nuclear Physics, Lomonosov Moscow State University, Moscow, Russia

7: Also at Universidade Estadual de Campinas, Campinas, Brazil

8: Also at Centre National de la Recherche Scientifique (CNRS) - IN2P3, Paris, France

-
- 9: Also at Laboratoire Leprince-Ringuet, Ecole Polytechnique, IN2P3-CNRS, Palaiseau, France
 - 10: Also at Joint Institute for Nuclear Research, Dubna, Russia
 - 11: Also at British University in Egypt, Cairo, Egypt
 - 12: Now at Suez University, Suez, Egypt
 - 13: Also at Cairo University, Cairo, Egypt
 - 14: Also at Fayoum University, El-Fayoum, Egypt
 - 15: Also at Université de Haute Alsace, Mulhouse, France
 - 16: Also at Tbilisi State University, Tbilisi, Georgia
 - 17: Also at RWTH Aachen University, III. Physikalisches Institut A, Aachen, Germany
 - 18: Also at University of Hamburg, Hamburg, Germany
 - 19: Also at Brandenburg University of Technology, Cottbus, Germany
 - 20: Also at Institute of Nuclear Research ATOMKI, Debrecen, Hungary
 - 21: Also at Eötvös Loránd University, Budapest, Hungary
 - 22: Also at University of Debrecen, Debrecen, Hungary
 - 23: Also at Wigner Research Centre for Physics, Budapest, Hungary
 - 24: Also at Indian Institute of Science Education and Research, Bhopal, India
 - 25: Also at University of Visva-Bharati, Santiniketan, India
 - 26: Now at King Abdulaziz University, Jeddah, Saudi Arabia
 - 27: Also at University of Ruhuna, Matara, Sri Lanka
 - 28: Also at Isfahan University of Technology, Isfahan, Iran
 - 29: Also at University of Tehran, Department of Engineering Science, Tehran, Iran
 - 30: Also at Plasma Physics Research Center, Science and Research Branch, Islamic Azad University, Tehran, Iran
 - 31: Also at Laboratori Nazionali di Legnaro dell'INFN, Legnaro, Italy
 - 32: Also at Università degli Studi di Siena, Siena, Italy
 - 33: Also at Purdue University, West Lafayette, USA
 - 34: Also at International Islamic University of Malaysia, Kuala Lumpur, Malaysia
 - 35: Also at Malaysian Nuclear Agency, MOSTI, Kajang, Malaysia
 - 36: Also at Consejo Nacional de Ciencia y Tecnología, Mexico city, Mexico
 - 37: Also at Warsaw University of Technology, Institute of Electronic Systems, Warsaw, Poland
 - 38: Also at Institute for Nuclear Research, Moscow, Russia
 - 39: Now at National Research Nuclear University 'Moscow Engineering Physics Institute' (MEPhI), Moscow, Russia
 - 40: Also at St. Petersburg State Polytechnical University, St. Petersburg, Russia
 - 41: Also at California Institute of Technology, Pasadena, USA
 - 42: Also at Faculty of Physics, University of Belgrade, Belgrade, Serbia
 - 43: Also at INFN Sezione di Roma; Università di Roma, Roma, Italy
 - 44: Also at National Technical University of Athens, Athens, Greece
 - 45: Also at Scuola Normale e Sezione dell'INFN, Pisa, Italy
 - 46: Also at National and Kapodistrian University of Athens, Athens, Greece
 - 47: Also at Institute for Theoretical and Experimental Physics, Moscow, Russia
 - 48: Also at Albert Einstein Center for Fundamental Physics, Bern, Switzerland
 - 49: Also at Adiyaman University, Adiyaman, Turkey
 - 50: Also at Mersin University, Mersin, Turkey
 - 51: Also at Cag University, Mersin, Turkey
 - 52: Also at Piri Reis University, Istanbul, Turkey
 - 53: Also at Gaziosmanpasa University, Tokat, Turkey
 - 54: Also at Ozyegin University, Istanbul, Turkey
 - 55: Also at Izmir Institute of Technology, Izmir, Turkey

- 56: Also at Marmara University, Istanbul, Turkey
- 57: Also at Kafkas University, Kars, Turkey
- 58: Also at Istanbul Bilgi University, Istanbul, Turkey
- 59: Also at Yildiz Technical University, Istanbul, Turkey
- 60: Also at Hacettepe University, Ankara, Turkey
- 61: Also at Rutherford Appleton Laboratory, Didcot, United Kingdom
- 62: Also at School of Physics and Astronomy, University of Southampton, Southampton, United Kingdom
- 63: Also at Instituto de Astrofísica de Canarias, La Laguna, Spain
- 64: Also at Utah Valley University, Orem, USA
- 65: Also at University of Belgrade, Faculty of Physics and Vinca Institute of Nuclear Sciences, Belgrade, Serbia
- 66: Also at Facoltà Ingegneria, Università di Roma, Roma, Italy
- 67: Also at Argonne National Laboratory, Argonne, USA
- 68: Also at Erzincan University, Erzincan, Turkey
- 69: Also at Mimar Sinan University, Istanbul, Istanbul, Turkey
- 70: Also at Texas A&M University at Qatar, Doha, Qatar
- 71: Also at Kyungpook National University, Daegu, Korea